The Astrophysical Journal, 654:606–624, 2007 January 1

THE EFFECT OF INTERNAL DISSIPATION AND SURFACE IRRADIATION ON THE STRUCTURE OF DISKS AND THE LOCATION OF THE SNOW LINE AROUND SUN-LIKE STARS

P. Garaud and D. N. C. Lin
Department of Applied Mathematics and Statistics, Baskin School of Engineering, University of California, Santa Cruz, CA;
and Department of Astronomy and Astrophysics, University of California, Santa Cruz, CA
Received 2006 May 3; accepted 2006 August 15

ABSTRACT

In theory of accretion disks, angular momentum and mass transfer are associated with the generation of energy through viscous dissipation. In the construction of SED models of protostellar disks, the stellar irradiation is usually assumed to be the dominant heating source. Here we construct a new set of self-consistent analytical disk models by taking into account both sources of thermal energy and the thermal structure of the disk across the midplane. We deduce a set of general formulae for the relationship between the mass accretion rate and the surface density profile. We apply it to determine the structure of protostellar disks under a state of steady accretion and derive the radial distribution of surface density and midplane temperature. The incorporation of the viscous heating in our model reduces the disk flaring angle and leads to lower photospheric temperatures than previously thought. Around T Tauri stars, the snow line can evolve from outside 10 AU during FU Orionis outbursts, to 2 AU during the quasi-steady accretion phase, to 0.7 AU when the accretion rate falls to about $10^{-9}\ M_\odot\ \mathrm{yr}^{-1}$, and finally reexpand beyond 2.2 AU during the protostellar-to-debris disk transition. The nonmonotonous evolution of the snow line may lead to the observed isotopic composition of water on both Venus and Earth. We also infer the presence of a marginally opaque, isothermal region with a surface density distribution similar to that of the MSN model. With a 40% higher temperature than that in the region immediately within, this transition may lead to an upturn in the SEDs in the MIR (24–70 μm) wavelength range. The optically thin, outermost regions of the disk have a shallow surface density profile of the dust that is consistent with millimeter observations of spatially resolved disks.

Subject headings: accretion, accretion disks — methods: analytical — solar system: formation

1. INTRODUCTION

The coplanar orbits of the planets around the Sun inspired Laplace (1796) to postulate the nebula hypothesis for solar system formation. The first evidence for these long anticipated protostellar disks was inferred from continuum IR emission at a level well above the stellar blackbody spectrum for a large fraction of stars in young clusters (Adams et al. 1987). Some flattened structures have also been resolved with millimeter imaging (Beckwith & Sargent 1996). The IR and millimeter excess emissions are attributed to the reprocessing of stellar light by dust grains. Since these disks are assumed to be the cradle of planet formation, the determination of their structure and evolution has been a central task in the quest to reconstruct the origin of planetary systems.

Obtaining accurate models of the thermodynamical structure of protostellar disks is important from both observational and theoretical points of view. First, while spatially resolved observations are possible for disks around nearby stars, the majority of the available data are in the form of spectral energy distributions (SEDs) and can only be fully interpreted with a thorough understanding of the underlying disk properties. Second, the details of the interaction between the gas and the condensed heavy elements (in any form from dust grains to planets) depend sensitively on the temperature and pressure gradient of the gas within the nebula. In short, to understand both observationally and theoretically the processes associated with planetary formation requires first and foremost a better understanding of the basic disk structure. This is the task we set out to do in this paper.

1.1. *Disk SEDs and Grain Properties*

In recent years, multiwavelength observations have provided a rich data bank of SEDs for most of the young stellar objects within several nearby clusters (see Lada et al. 2006). Detailed numerical modeling in terms of reprocessed stellar irradiation has been successful in reproducing observations (Chiang & Goldreich 1997, hereafter CG97; Bell 1999; D'Alessio et al. 2001; Calvet et al. 2002; Dullemond & Dominik 2004). These analyses show that SEDs are particularly sensitive to three properties of the disks: (1) the nature of the dust grains (density, size distribution, physical and chemical composition), (2) the thermal and chemical structure of the gas, and (3) the global geometrical structure of the disk such as the inclination, degree of flaring, size, and presence/absence of a hole (Dullemond et al. 2006).

Current models of dust particles in disks usually assume that they have the same power-law size distribution as that of the interstellar grains (Mathis et al. 1977), but with varying upper and lower cutoffs. This power law of the Mathis et al. (1977) distribution implies that the total cross-sectional area is dominated by the contribution from the smallest grains (below micron size) whereas the large grains (>1 mm) contain most of the solid-phase mass of heavy elements. Consequently, the disk SEDs in the wavelength range observed by *Spitzer* are most sensitive to the small grains, which are tightly coupled to the gas both thermally and dynamically.

The objective of this paper is to construct a set of comprehensive analytical models of the thermodynamical structure of the disks, which can easily be utilized for the statistical analysis of large SED data sets and a more physical interpretation of the planet formation environment.

1.2. *Gas-Dust Interaction*

In parallel with the observational aspects of the study of the disk SEDs, large theoretical efforts have recently been deployed toward understanding the growth of small grains and the motion of the larger particles (and small planetesimals) within the primordial

solar nebula (Weidenschilling 1977; Weidenschilling & Cuzzi 1993). The properties of the dust grains have recently been thoroughly studied since evidence for dust growth (D'Alessio et al. 2001; Shuping et al. 2003; McCabe et al. 2003) or local (spatial) accumulation (Greaves et al. 2005) could be the first signs of ongoing planet formation.

While the tiniest dust grains are dynamically very strongly coupled with the gas and largely follow its evolution, intermediate-size objects ("pebbles" to "boulders") have a different intrinsic motion that is sensitively dependent on the structure (temperature, pressure gradient) and dynamical nature (turbulent vs. laminar) of the nebular gas (Morfill & Voelk 1984; Supulver & Lin 2000; Youdin & Chiang 2004; Ciesla & Cuzzi 2006).

It is thought that gas drag causes meter-sized objects to spiral into the central star within a few hundred orbital periods (Adachi et al. 1976), but the ubiquitous presence of planets around at least 10% of all observed stars (Marcy et al. 2000) suggests the existence of a reliable yet still unidentified mechanism for the retention of at least a few percent of the total content of heavy elements passing through the nebula. Meanwhile, upper limits on this retention efficiency have independently been set through the observed homogeneity of the heavy-element abundances among Sun-like stars in older clusters such as the Pleiades (Wilden et al. 2002), the Hyades (Quillen 2002), and IC 4665 (Shen et al. 2005). These studies suggest that the total mass of heavy elements retained by the protostellar disks toward planet formation is at most a few times that contained in a minimum solar nebula (MSN; Hayashi et al. 1985).

A self-consistent model of the thermal structure of protostellar disks is essential to understand these rather strongly constrained estimates of the heavy-element retention efficiency during planet formation.

1.3. *Protostellar Disk Models*

The thermal structure of the gas is determined by a balance between the generation of heat (through stellar irradiation [Adams et al. 1987] and viscous dissipation [Lynden-Bell & Pringle 1974]), its transport (through radiative diffusion and advective transport), and finally cooling (through emission by the gas itself, or more importantly by the dust grains with which the gas is thermally connected). In existing analytical models of protostellar disks, the energy source is usually attributed to either viscous dissipation (Lin & Papaloizou 1980, 1985; Ruden & Lin 1986) or stellar irradiation (Adams et al. 1987; CG97). More recently, numerical models of the disks have begun to take both sources into account (Bell 1999; d'Alessio et al. 2001; Dullemond & Dominik 2004).

In this paper we propose a new simple kind of analytical model to calculate the two-dimensional (r, z) thermal structure of the disk, taking into account both energy sources. The nature of the model enables us to derive analytical formulae for all of the disk quantities and derive scaling relations between the disk properties and the host star properties.

Our work is largely inspired by CG97. As they suggest, most of the stellar radiation is intercepted by a superheated layer of grains that reemits part of it toward the disk midplane. We also adopt an isothermal structure in the optically thin regions above the disk photosphere (in the case where the midplane is optically thick) and in the marginally opaque or optically thin outer regions of the disk. However, we introduce two major modifications to their work.

First, we model the optically thick regions in more detail by considering their nonisothermal structure. A warmer midplane is a natural consequence of heating by viscous dissipation (in the case of optically thick disks) combined with down-gradient transport toward the photosphere. We assume a polytropic structure for the disk stratification in the direction across the midplane. This assumption can be shown to be consistent with some possible heat generation and transport mechanisms, as for instance in the case of viscously heated convectively unstable disks. It can also naturally be considered an approximation to the true stratification of the disk, with a polytropic index to be chosen from best fits of numerical simulations.

Radiative heating by the central star is well known to be the dominant heat source throughout most disks; nonetheless, for completeness we also consider regions of the disk in which the dominant heating process is through viscous heating, which naturally occurs close to the central star. While this effect is not particularly important for classical T Tauri stars ($\dot{M} < 10^{-7}\,M_{\odot}\,\mathrm{yr}^{-1}$) outward of 1 AU, the viscously dominated region can extend up to tens of AU for much larger mass accretion rates.

Second, while CG97 specifically assumed an MSN surface density profile ($\Sigma_{\mathrm{MSN}} = 1000 r_{\mathrm{AU}}^{-3/2}$ g cm^{-2}), we derive instead self-consistent formulae between the disk structure and the mass accretion rate. The evolution of the disk can then be studied for a set of arbitrary initial and boundary conditions if desired. In this paper we restrict our study to the case of steady accretion (with a radially constant $\dot{M}$) for the sake of simplicity. While still being an idealized assumption, this is the state toward which accretion disks relax should a constant supply of material be provided near their outer rim. Consequently, it is a better approximation to the disk structure for the inner regions of the disk (and presumably out to a few hundred AU; Lin & Papaloizou 1980, 1985) than the standard MSN power-law surface density profile usually used.

1.4. *The Importance of the Snow Line*

The temperature of a typical T Tauri disk decreases from over 1000 K within a fraction of 1 AU to well below 100 K beyond 10 AU (see § 6). In the low pressure and tenuous environment of protostellar disks, ice grains sublimate between 150 and 170 K. The snow line is generally defined to be the location where the gas temperature attains these values (Hayashi et al. 1985).

As an example of the potential of the new disk model we propose, we present new results on the evolution of the snow line around solar-type T Tauri stars. This analysis is much more than an academic exercise, however, since the snow line is thought to play a very important role in the formation of planets.

The presence of a snow line somewhere in the disk separates regions primarily containing refractory silicates from those containing volatile ices. Since the relative abundance of the lighter elements is at least a factor of 4 larger than that of metals, the supply of grains as planet-building materials is much richer beyond the snow line. The large difference between the typical radial velocity of heavy elements in condensed form and in gaseous form suggests the possibility of accumulation of material near the snow line (Takeuchi & Lin 2005; Ciesla & Cuzzi 2006). The thermal "anomaly" in the disk structure caused by the presence of the snow line may also be associated with a flattening of the pressure gradient, which could slow down the radial migration of the larger particles and further enhance the local accumulation of material. Finally, this boundary may separate the domain of terrestrial planet versus gas giant planet formation (Ida & Lin 2004).

Observational evidence for the presence of a snow line in disks around other stars is scarce. Measurements of the location of the snow line in the protosolar nebula have been inferred from the actual water content and suggestions of aqueous alteration in various families of meteorites (Lunine 2005) to be between 2.5 and 3 AU, within the asteroid belt.

We show that while our model naturally reproduces its current location, it also predicts large excursions in the position and extent of the snow line during the early stages of the protosolar nebula. We discuss the consequences of these findings for the formation and hydration of planets in our solar system.

1.5. *Outline of the Paper*

The paper is organized as follows. In § 2 we briefly recapitulate the total energy balance in the disk as a function of the dominant heating and cooling processes. We largely follow the footsteps of CG97 except where explicitly mentioned. In particular, we use their prescription for the absorption and emission properties of the dust grains, which are both sensitively dependent on the typical wavelength of the photons considered. This leads to a complex vertical and radial structure of the disk, which is also presented in § 2.

In §§ 3 and 4 we derive analytical formulae for the density and temperature profile in each of the layers for each of the regions considered and deduce the two-dimensional structure of the disk. The methodology followed consists in calculating the position of the superheated dust grains as a function of the total optical depth of the disk, deducing the flaring angle of the disk and the associated intercepted stellar flux, and equating it with the energy lost through radiation to deduce the thermal structure of the disk. Once obtained, we can then evaluate the mass accretion rate. In the steady state accretion approximation, the constant mass accretion rate assumed is then used to calculate the total surface density of the disk and to deduce the total optical depth that closes the system of equations. Naturally, some of these steps are simplified in the isothermal case and in the case where the dominant energy source is viscous heating. By following this method, we ensure that the disk structure is determined in a self-consistent manner.

In § 5 we estimate analytically the location of various critical radii as a function of the accretion rate and the mass of the central star. These radii include those separating the radiatively dominated optically thin, marginally opaque, optically thick, and finally viscously dominated regions of the disk. We also obtain a rough estimate of the radial location of the snow line from the radius below which the disk midplane temperature exceeds 160 K.

In § 6 we apply our prescription to compute the structure of disks with a range of accretion rates around T Tauri stars. We confirm that throughout most of the disk, the flaring angle in a steady state accretion state increases with radius. In the optically thin region, we recover the scalings of CG97 for the temperature and scale height profiles, since these are independent of mass accretion rate. However, our surface density profile falls off with radius much less steeply (as r^{-1}) than that assumed for the MSN. This finding is consistent with recent observations of spatially resolved disks (Mundy et al. 2000; Looney et al. 2003). In the marginally opaque region, we also coincidentally recover the scalings of CG97 since our model predicts in this region a surface density profile varying as that of the MSN. The temperature is interestingly found to be significantly larger than in the optically thick region just within; thus, we predict the existence of a "hot ring" at radii ~20–30 AU around classical T Tauri stars. In the optically thick regions our model predicts a significantly flatter disk, with notable consequences on the surface density, photospheric temperature profile, and the position of the snow line. We deduce three important results: the snow line can be very extended, it has a largely nonmonotonic evolution, and it can move (for a solar-type T Tauri star) as far in as the current orbit of Venus.

Finally, we discuss the assumptions of the model in § 7, as well as its implications for planetary formation and observations of protostellar disks.

2. BASIC MODEL ASSUMPTIONS AND METHODOLOGY

2.1. *Basic Framework*

Our model follows a standard 1+1D methodology, which implicitly assumes that the disk is thin, with independent vertical (i.e., normal to the disk plane) and radial structures. The dust, which largely governs the thermal structure, is initially assumed to be fully mixed with the gas; this assumption will be relaxed in future work. In the present context, we adopt a prescription in which

$$\rho_d = Z\rho, \tag{1}$$

where ρ is the gas density, ρ_d is the dust density, and the "metallicity" Z is in principle a slowly varying function of radius and time. However, note that the magnitude of Z may change abruptly near transition fronts (e.g., it decreases by a factor of 4 as ice grains cross the sublimation line). We will consider the details of the disk structure near the snow line in a follow-up paper. In addition, note that ρ_d refers to the heavy-element mass density contained in small particles only (with settling times that are much larger than the turbulent diffusion time); there could be a significant fraction of "undetectable" heavy elements condensed in larger size objects, which the model presented here neglects.

The disk has two principal thermal energy sources: radiative heating (from the central star) and viscous heating (from turbulent dissipation associated with momentum transport). In intermediate and outer regions of typical disks around T Tauri stars, radiative heating is by far the largest contribution to the total energy budget and essentially determines the thermal properties of both the grains and the gas in the disk. In optically thick regions, even when radiative heating dominates the *total* energy budget, viscous heating plays an important role in maintaining a warmer midplane layer and determines the vertical stratification of the disk. Finally, much closer to the central star, viscous dissipation becomes the main agent in heating the disk.

The effectiveness of the conductive thermal coupling between the gas and the dust is crucial to the determination of the disk structure. This coupling depends essentially on the wavelengths considered, as well as on the collision timescale between the dust particles and the gas molecules. CG97 discussed these processes in their seminal work; we will not repeat them here.

For computational convenience and reasonable accuracy, we assume as they do that the emissivity and opacity of the grains interacting with a blackbody photon spectrum peaked at temperature T_i are

$$\epsilon_i = \left(\frac{T_i}{T_\star}\right)^\beta, \quad \kappa_i = \kappa_V \left(\frac{T_i}{T_\star}\right)^\beta. \tag{2}$$

When applying the model to T Tauri stars (see § 6), we adopt the value $\beta = 1$ although all of the formulae are given for arbitrary values of β. In the same spirit, we also adopt the approximate value of $\kappa_V = 1\ \mathrm{cm^2\ g^{-1}}$ suggested by the work of d'Alessio et al. (2001).

2.2. *Layered Structure of the Disk*

Following the model of CG97 (also recently developed by Rafikov & De Colle 2006), we identify several layers in a typical disk. The detailed structure of these layers in various disk regions is schematically illustrated in Figure 1.

The top layer of the disk is referred to as layer 1 where the grains are directly exposed to the stellar photons. Since submillimeter-size

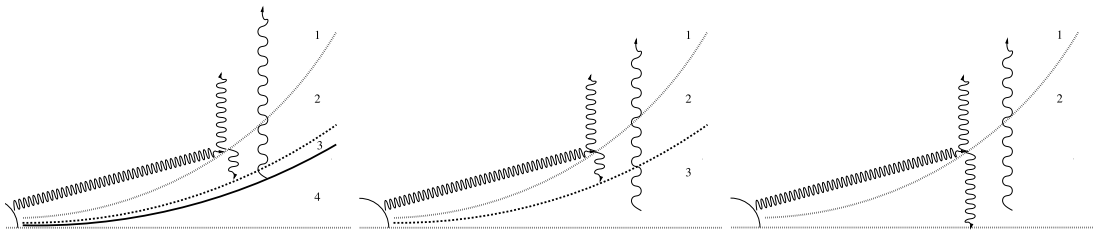

FIG. 1.—Cartoon representation of the layered model for the three regions considered. *Left to right*: Optically thick, marginally opaque, and optically thin cases. In all regions, the top layer (layer 1) contains superheated grains directly exposed to the (mostly visible) radiation from the central star. Its lower boundary (*dotted line*) is referred to as $z_s(r)$ and is calculated by setting the optical depth from the central star to the line to unity (see the Appendix). The superheated grains reradiate in the IR both toward infinity and toward the midplane. Some of the midplane grains are directly irradiated by the reprocessed light from the superheated grains (layer 2). In the optically thick and marginal cases, however, part of the midplane (layer 3) is optically thick to this emission. Grains in layers 2 and/or 3 in turn reprocess the absorbed light and reemit it at slightly longer wavelengths still toward infinity. When the disk is optically thick to its own emitted IR light, a fourth layer is constructed, and the emission occurs from the photosphere (*solid line*) located at $z_e(r)$. Note that unless the fourth layer is entirely absent, layer 3 is very thin and can be neglected.

dust grains are inefficient radiators at IR wavelengths and dust-gas collisions are too scarce to account for significant cooling, grains in layer 1 are "superheated" to a temperature T_s satisfying roughly

$$\frac{L_\star}{4\pi r^2} = 4\epsilon_s \sigma T_s^4, \tag{3}$$

where $L_\star$ is the stellar luminosity, r is the distance from the central star, T_s is the temperature of the superheated dust grains, and ϵ_s is their emissivity at that temperature.

The energy balance in equation (3) is valid as long as the grains are directly heated by the central star. Thus, layer 1 extends from the central star outward until a visual optical depth 1 is reached (*dotted line*). The temperature of the gas in this layer is difficult to determine without a complete description of the (dynamical, thermal, and chemical) interaction between the dust grains, the H_2 molecules, and the coolant molecules (such as H_2O and others). However, the gas temperature in layer 1 has relatively little impact on the vertical stratification of the lower regions of the disk, and for simplicity we set it to either the temperature near the midplane T_m (in the optically thin case) or the effective temperature of the disk T_e (in the optically thick case).

Superheated dust grains reradiate half of the absorbed flux toward infinity and half toward the disk midplane. Where this radiation is absorbed depends on the optical depth of the midplane layer to reprocessed IR photons. Thus, we construct layers 2 and 3 where layer 2 is optically thin to the radiation emitted by the superheated dust grains, while layer 3 is optically thick to it (note that layer 3 only exists for large enough surface density). The two layers are separated by the dashed line, defined as the position where the optical depth of the grains to the radiation from the superheated layer reaches unity on a path perpendicular to the midplane.

Finally, the heated midplane grains reemit toward infinity at some temperature lower than T_s still. Again, the total outgoing flux depends on the optical depth of the midplane to its own emission: if the surface density is large enough, the disk is optically thick to its own emission and we construct a fourth layer (layer 4) delimited by the photosphere (*solid line*). At the photosphere, the disk emits a blackbody spectrum with temperature T_e, which is always lower than T_s. Owing to the difference between T_e and T_s, there exists a small difference between the midplane layer photosphere (*solid line*) and the edge of layers 2 and 3 (*dashed line*). While this difference is usually negligible (and neglected) when the inner disk is optically thick, there can exist an intermediate regime (also discussed by CG97) where the midplane layer is optically thin to its own radiation but optically thick to the radiation from the superheated layer; in this case, layer 4 vanishes. We refer to this region as the *marginally opaque* region. When the midplane layer is also optically thin to the superheated grains, layer 3 vanishes and we refer to this region as the *optically thin* region. Note that for even smaller total dust content, the whole disk becomes optically thin to the radiation from the central star. We do not model this last phase in this paper.

2.3. *Variation of the Layered Structure with Radius*

The total energy balance in the various radial regions of the disk is now described in more detail.

Optically thin disk regions.—In the low surface density regions, mostly at large disk radii, the entire midplane layer is optically thin to the radiation from the superheated grains, as well as to its own emission. In these regions, layers 3 and 4 vanish while layer 2 is preserved. The grains in the midplane (now layer 2) are heated by reprocessed radiation from the superheated grains located on both sides of the disk. As a result, both gas and individual dust grains have a temperature T_m given by

$$2\epsilon_s \frac{A_s}{2} \frac{L_\star}{4\pi r^2} = \epsilon_m \sigma T_m^4, \tag{4}$$

where A_s is the total emitting area filling factor of superheated grains above z_s (i.e., the fraction of solid angle covered by grains), T_m is the midplane temperature (the gas is assumed to be isothermal in this region), and ϵ_m is the corresponding emissivity. Note that the factor of ϵ_s on the left-hand side accounts for the fact that the grains are inefficient absorbers at IR wavelengths. We also include the additional factor of 2 accounting for the emission from both layers, which was neglected by CG97.

Marginally opaque disk regions.—In an intermediate range of surface density, the midplane layer is optically thick to the radiation from the superheated dust grains, but optically thin to its own emission. In this region, the disk is again assumed to be isothermal and layer 4 does not exist. Taking into account the energy budget for the entire disk, the grain and gas temperatures are determined by

$$\frac{A_s}{2} \frac{L_\star}{4\pi r^2} = \epsilon_m A_m \sigma T_m^4, \tag{5}$$

where A_m is the total area filling factor of grains in the midplane layer.

Opaque disk regions.—In the limit where the surface density is sufficiently large for the midplane layer to be optically thick to its own radiation, T_m cannot be directly determined from the stellar flux. The total energy budget determines instead the effective temperature T_e since the photosphere is reasonably close to the

location where the reprocessed radiation emitted by the superheated grains is deposited. Thus,

$$\frac{A_s}{2}\frac{L_\star}{4\pi r^2} = \sigma T_e^4, \tag{6}$$

where T_e is the temperature (of both dust and gas) at the photosphere. Note that this equation assumes that the contribution from viscous heating is negligible, which can be shown to be valid outward of about 1 AU for a typical T Tauri star. If we are interested only in regions outward of the snow line anyway, this approximation is justified. However, in the innermost region of the disk where viscous dissipation is the dominant heating mechanism the total energy budget becomes

$$\frac{3}{4\pi}\dot{M}\Omega_{\rm K}^2 = 2\sigma T_e^4 \tag{7}$$

instead, where $\dot{M}$ is the local mass accretion rate and $\Omega_{\rm K}$ is the local Keplerian angular velocity. This equation relates the total energy generated by viscous dissipation within the disk midplane to the emitted flux on both sides of the disk.

2.4. *Radial Power Law: Notations*

For simplicity, in each of the four regions, we write the midplane quantities as

$$T_m(r) = \overline{T} r_{\rm AU}^q, \tag{8}$$

$$\rho_m(r) = \overline{\rho} r_{\rm AU}^p, \tag{9}$$

where here and in all that follows we set $r_{\rm AU} = r/(1\ {\rm AU})$. This uniquely defines the indices p and q, in a manner consistent with the notation of Takeuchi & Lin (2002). The resulting isothermal disk scale height is therefore obtained as

$$h(r) = \overline{h} r_{\rm AU}^{(q+3)/2}. \tag{10}$$

Note that $q > -1$ corresponds to a flaring disk, whereas $q < -1$ corresponds to a self-shadowed disk. In all that follows, we assume that the disk is flaring and check this assumption for self-consistency. The disk surface density profile is

$$\Sigma = \overline{\Sigma} r_{\rm AU}^{-s}. \tag{11}$$

For instance, one can set $s = 3/2$ to recover the MSN model. For a steadily accreting disk, on the other hand, we determine Σ from the requirement that the total mass accretion rate $\dot{M} = 3\pi\nu_t\Sigma$ be constant with radius, where we have adopted a standard α-prescription for the eddy viscosity ν_t with value

$$\nu_t = \alpha_t c_m h. \tag{12}$$

In that case

$$s = q + \frac{3}{2}, \tag{13}$$

$$\overline{\Sigma} = \frac{\dot{M}}{3\pi\alpha_t}\frac{(1\ {\rm AU})^{3/2}}{\sqrt{\gamma G M_\star}\,\overline{h}^2}. \tag{14}$$

3. STRUCTURE OF OPTICALLY THIN AND MARGINAL DISK REGIONS

In the outer regions of the disk, the total surface density of grains is sufficiently low for the disk to be optically thin to its own radiation. In this case, layer 4 vanishes. We assume, as in CG97, that the gas is isothermal in the direction normal to the plane of the disk and has a temperature T_m.

Integrating the equation for hydrostatic equilibrium yields the standard Gaussian vertical density distribution for the gas:

$$\rho(r, z) = \rho_m(r)\exp\left[-\frac{z^2}{2h^2(r)}\right], \quad h^2 = \frac{c_m^2}{\gamma\Omega_{\rm K}^2} = \frac{R_g T_m}{\mu\Omega_{\rm K}^2}, \tag{15}$$

where c_m is the sound speed for a gas at temperature T_m, with mean molecular weight μ and adiabatic index γ; R_g is the gas constant. When the dust and the gas are fully mixed, the interface z_s between layer 1 and layer 2 (which can be thought of as the position of the superheated dust layer) is obtained by solving the equation

$$\int_0^r \tilde{Z}\rho(r', z')\kappa_V\, d\boldsymbol{l} = 1 \tag{16}$$

on a straight path $d\boldsymbol{l}$ from the central star to the point (r, z_s) [namely, $z' = (z_s/r)r'$]. Here $\tilde{Z}$ is the assumed metallicity Z normalized to the value used for the determination of κ_V, namely, 1%. Thus, $\tilde{Z} = Z/0.01$. Note that it can also be regarded as $\sim 10^{[{\rm Fe/H}]}$, where [Fe/H] is the metallicity normalized with respect to that of the Sun. Assuming that the disk is flaring, one can approximate this equation using the variant of a stationary phase method (see the Appendix), which yields the equation (valid at every radius r within the region)

$$\tilde{Z}\rho_m h\kappa_V \exp\left(-\frac{z_s^2}{2h^2}\right) = \frac{z_s^2}{h^2}\alpha + \frac{h}{r}\frac{d\ln\left(\tilde{Z}\rho_m\right)}{d\ln r}, \tag{17}$$

where we have defined α as the grazing angle between the incoming radiation from the star and the local stratification:

$$\alpha = r\frac{d}{dr}\left(\frac{h}{r}\right). \tag{18}$$

Note that this approximation is only strictly valid in the limit where z_s is larger than a few scale heights. By inspection, one can note that the second term on the right-hand side of equation (17) is negligible within the same limit unless the disk has a sudden jump in gas density or metallicity (this could occur near a planet-induced gap, or near the successive sublimation zones). Deferring the study of these transition zones to a later paper, we find that the ratio z_s/h is otherwise given by

$$\frac{z_s}{h} = \left[2{\rm LambertW}\left(\frac{\tau_V^{\rm tot}}{\sqrt{2\pi}\alpha}\right)\right]^{1/2}, \tag{19}$$

where $\tau_V^{\rm tot} = \tilde{Z}\Sigma\kappa_V/2$ is the total visual optical depth from the midplane to infinity on a path perpendicular to the disk. Given that the disk is isothermal, $\Sigma = (2\pi)^{1/2}\rho_m h$.

Note that the LambertW function is defined as the inverse of the function $f(x) = x\exp(x)$, or in other words, if $y = x\exp(x)$, then $x = {\rm LambertW}(y)$. For ease of computation, and for large values of y (for y between 10 and 10^5, say), a fairly good approximation (to within about 10%) of the LambertW function is given by

$${\rm LambertW}(y) \simeq 0.8\ln(y). \tag{20}$$

This can be seen in Figure 2.

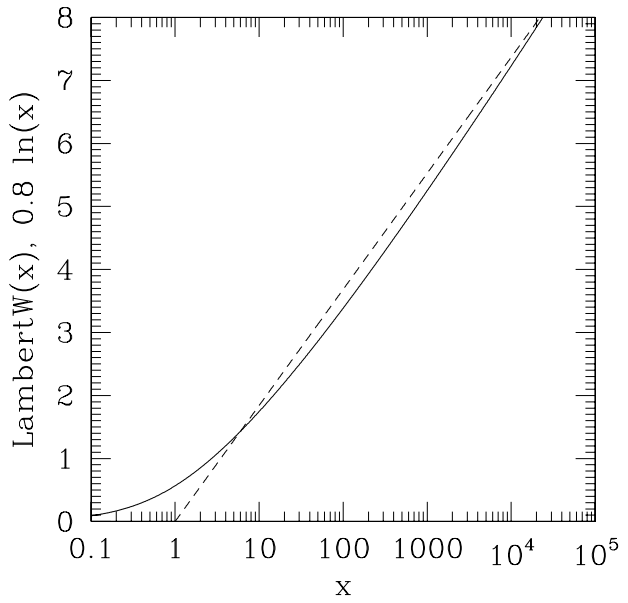

FIG. 2.—LambertW(x) function (*solid line*) and its approximation $0.8 \ln(x)$ (*dashed line*) for large values of x. Although this is not an asymptotic approximation and is not uniformly valid for $x \to \infty$, it is quite good in the range considered.

We therefore note that as long as $\tau_V^{\rm tot} \gg (2\pi)^{1/2}\alpha$ the ratio z_s/h is a slowly varying function of radius with

$$\frac{z_s}{h} = C(r) \simeq \left[3.7 \log_{10}\left(\frac{\tau_V^{\rm tot}}{\sqrt{2\pi}\alpha}\right)\right]^{1/2}. \tag{21}$$

Calculating $C(r)$ exactly in the case of a classical T Tauri star reveals that C varies between 3 and 4 in the outer regions of the disk, confirming the *Ansatz* ($z_s \simeq 4h$) of CG97. However, for other stellar types or for other mass accretion rates, we find that the superheated dust layer position varies widely (with C taking any value between 1 and 6).

Once the magnitude of z_s is determined, we need to identify the surface area filling factor A_s of the reprocessing material contained within the superheated layer, which is equal to the visual optical depth τ_V^s. This is done through the integral

$$A_s \simeq \int_{z_s}^{\infty} \tilde{Z}\rho\kappa_V \, dz = \tau_V^s. \tag{22}$$

Using the same stationary phase approximation (see the Appendix), we evaluate the integral to get

$$A_s \simeq \tilde{Z}\rho_m\kappa_V h \exp\left(-\frac{z_s^2}{2h^2}\right)\frac{h}{z_s}, \tag{23}$$

and combining this with equation (17) yields

$$A_s \simeq \frac{z_s}{h}\alpha. \tag{24}$$

Note that this expression differs from the one suggested by CG97 by a geometrical factor of $z_s/h = C(r)$; this difference arises in choosing to determine A_s from a path that is perpendicular to the midplane rather than perpendicular to the disk stratification. We prefer the former interpretation as more consistent with the 1+1D assumption, although the latter is also acceptable within the degree of approximation associated with this analytical approach.

3.1. *Optically Thin Disk Regions*

To compute the radial structure of the disk, we combine equations (4), (24), and (18) and ignore the slow dependence in r of $C(r)$. This derivation yields an equation for $h(r)/r$, for instance, of the general form described and solved in the Appendix:

$$\frac{d}{dr}\left(\frac{h}{r}\right) = \frac{2^{2\beta/4+\beta}}{C}\left(\frac{\mu}{R_g}\frac{GM_\star}{T_\star}\right)^{4+\beta} R_\star^{-(4\beta+8)/(4+\beta)} h^{8+2\beta} \times r^{(3\beta+4)/(4+\beta)-3(4+\beta)}, \tag{25}$$

which can be integrated to yield equation (10) with

$$\frac{\overline{h}}{\rm AU} = \left[\frac{2^{2\beta/4+\beta}}{C}\frac{2\beta^2+15\beta+28}{\beta^2+4\beta+8}\left(\frac{\mu}{R_g}\frac{GM_\star}{R_\star T_\star}\right)^{4+\beta}\right]^{-1/(7+2\beta)} \times \left(\frac{R_\star}{1\ {\rm AU}}\right)^{-(8+4\beta+\beta^2)/(28+15\beta+2\beta^2)},$$

$$\frac{q+3}{2} = \frac{\beta^2+4\beta+8}{2\beta^2+15\beta+28} + 1. \tag{26}$$

If $\beta = 1$, then $q = -19/45$, with $h \propto r_{\rm AU}^{58/45}$ and the flaring angle $\alpha \propto r_{\rm AU}^{13/45}$. This result is independent of the surface density distribution of the gas and is similar (within factors of order unity) to the expression derived by CG97. If we require in addition that the disk be in a state of steady accretion, the surface density distribution can be deduced directly from equation (11), and in that case $s = 97/90 \simeq 1$. This result is particularly interesting in the light of the observational results of Mundy et al. (2000), who found that the surface density profile of spatially resolved disks varied as $r_{\rm AU}^{-1}$ rather than $r_{\rm AU}^{-3/2}$.

This analysis is only valid in the region delimited from the inside by the inequality $\tau_s^{\rm tot} < \frac{2}{3}$ (where $\tau_s^{\rm tot} = \tilde{Z}\Sigma\kappa_s/2$), and from the outside by the inequality $\tau_V^{\rm tot} \gg \alpha$ (or $h \simeq r$, whichever happens closest to the central star). Note that as the total optical depth drops below α, the superheated layer becomes progressively more and more optically thin to the radiation from the central star. This is expressed mathematically by $C \to 0$. When this happens, all of the grains directly exposed become "superheated." The temperature of the gas, however, is more difficult to evaluate because of the long collision timescale between grains and gas molecules; as a result, it is unclear whether the disk retains its flaring structure or becomes self-shadowed, although we suspect that the latter is more likely. This transition would appear as an outer edge to the observable disk.

In addition, when considering the case of steady state accretion, it is important to bear in mind the underlying assumptions that (1) the disk has time to relax to the quasi–steady state and (2) a constant mass supply is indeed provided to the disk from the outer rim. Both of these assumptions are difficult to justify beyond a few hundred AU.

3.2. *Marginally Opaque Disk Regions*

To compute the radial structure in the marginally opaque case, we need to determine the emitting surface of grains in the midplane region $z \in [0, z_s]$, which is very well approximated by $\tau_V^{\rm tot}$

in the limit where z_s is larger than a few scale heights (which we proved to be self-consistently true):

$$A_m \simeq \tau_V^{\rm tot} = \frac{\tilde{Z}\Sigma\kappa_V}{2}. \quad (27)$$

Using the same method as in the previous section (which involves using eqs. [5], [24], and [27]), we find that the disk scale height is

$$\frac{\overline{h}}{1\ {\rm AU}} = \left[\frac{2}{C}\frac{7+2\beta}{2+s+\beta}\frac{\tilde{Z}\overline{\Sigma}\kappa_V}{2}\left(\frac{\mu}{R_g}\frac{GM_\star}{R_\star T_\star}\right)^{4+\beta}\right]^{-1/(7+2\beta)} \times \left(\frac{R_\star}{1\ {\rm AU}}\right)^{-(2+\beta)/(7+2\beta)},$$
$$\frac{q+3}{2} = \frac{9+s+3\beta}{7+2\beta}. \quad (28)$$

Interestingly, we find that the MSN scaling law is the one consistent with steady accretion, with $h \propto r_{\rm AU}^{3/2}$ and

$$s = \frac{3}{2}, \quad q = 0, \quad \alpha = \frac{h}{2r}, \quad (29)$$

for any value of β. This value of q implies that the disk is radially isothermal in this region. In addition, $\overline{\Sigma}$ and $\overline{h}$ are obtained by solving simultaneously equations (28) and (14), so that

$$\frac{\overline{h}}{1\ {\rm AU}} = \left[\frac{2}{C}\frac{\dot{M}\tilde{Z}\kappa_V}{3\pi\alpha_t\sqrt{\gamma GM_\star R_\star}}\left(\frac{\mu}{R_g}\frac{GM_\star}{R_\star T_\star}\right)^{4+\beta}\right]^{-1/(5+2\beta)} \times \left(\frac{R_\star}{1\ {\rm AU}}\right)^{-1/2}, \quad (30)$$

and the value of the radially constant temperature is

$$T_m = \frac{\mu}{R_g}\frac{GM_\star}{(1\ {\rm AU})^3}\overline{h}^2. \quad (31)$$

Again, this result recovers the expression obtained by CG97. The marginally opaque region terminates at the radius where $\tau_m^{\rm tot} = \frac{2}{3}$, where $\tau_m^{\rm tot} = \tilde{Z}\kappa_m\Sigma/2$.

4. VERTICAL STRUCTURE OF OPAQUE DISK REGIONS

Disks are heated by both viscous dissipation and stellar irradiation. When the midplane is opaque to its own thermal radiation, heat generated near the midplane can only be transported toward the photosphere by turbulent or radiative down-gradient diffusion. This implies the emergence of a temperature gradient across the disk midplane, which must be calculated self-consistently.

4.1. *Thermal Stratification in the Optically Thick Layer*

Existing detailed disk models are constructed based on the numerical integration of this thermal equilibrium equation (see d'Alessio et al. 2001; Dullemond & Dominik 2004),

$$\rho\nu\left[r\frac{\partial\Omega_{\rm K}}{\partial r}\right]^2 = \nabla\cdot(F_{\rm rad} + F_{\rm turb}). \quad (32)$$

Unfortunately, the nonlinearities in the radiative contribution to the heat flux prevent simple analytical solutions. Instead, we adopt a polytropic structure for the disk, which can be either deduced exactly assuming idealized heat transport mechanisms (such as effective convective transport leading to an adiabatic stratification) or considered an approximation to the solution of the full transport equation.

Indeed, let us consider the standard polytropic equation

$$p = K\rho^{1+1/n}, \quad (33)$$

where p is the gas pressure, n is the polytropic index, and K is the polytropic constant. The equation of hydrostatic equilibrium across the midplane is

$$\frac{dp}{dz} = -\rho\Omega_{\rm K}^2 z, \quad (34)$$

where we have neglected the self-gravity of the disk. Combining these with a perfect gas equation of state

$$p = \frac{R_g\rho T}{\mu}, \quad (35)$$

where R_g is the gas constant and μ is the mean molecular weight, we obtain

$$T(r, z) = T_m(r)\left[1 - \frac{z^2}{H(r)^2}\right],$$
$$\rho(r, z) = \rho_m(r)\left[1 - \frac{z^2}{H(r)^2}\right]^n, \quad (36)$$

where H is uniquely related to the conventionally defined disk isothermal scale height

$$h^2 = \frac{c_m^2}{\gamma\Omega_{\rm K}^2} \quad (37)$$

(where γ is the adiabatic index for the gas) as

$$\frac{H}{h} = \theta = \sqrt{2n+2}. \quad (38)$$

The expression for the temperature given in equation (36) reveals part of the nature of the polytropic approximation: it is found to be the equivalent of a third-order accurate Taylor expansion of the true temperature profile in the variable z. It is interesting to note, however, that the fit is quite good even when $z \to H$. The normalizing quantities T_m and H are determined from the total integrated energy budget in the midplane layer (see below) and as such are relatively independent of this approximation, up to constants of order unity. The expression for the density profile, on the other hand, contains the polytropic index n. In the case of convective, adiabatically stratified disks we choose n such that $\gamma = 1 + 1/n$. If the gas is composed of mostly molecular hydrogen with a solar composition,

$$\gamma = 1.4, \quad \mu = 2.4, \quad (39)$$

then $n = 2.5$. In the case of radiative disks, or disks with mixed heat transport mechanisms, n must be chosen in such a way as to provide the best fit with numerically integrated solutions. It has been suggested that for purely radiative disks, one may consider choosing for simplicity $n \simeq 3 - \beta$ (G. Ogilvie 2005, private communication).

Note also that H determines the location where, in principle, both the gas density and temperature would drop to zero. However, this midplane solution is only valid within the optically

thick interior of the disk, i.e., within the interval $z \in [0, z_e(r)]$, where $z_e(r)$ is the position of the photosphere. For the convenience of the following discussions, we define the ratio

$$\Delta_e = z_e/H. \tag{40}$$

Above the photosphere, the temperature and density profiles are matched onto an isothermal atmosphere solution with the photospheric temperature T_e. The matching procedure involves solving the total energy equation to determine T_e, which then uniquely yields the values of the midplane temperature and density T_m and ρ_m. In order to do this, we must first determine the position of the photosphere, which can be done once the vertical stratification in the atmosphere is calculated.

4.2. *Disk Atmosphere*

Above the photosphere, we assume the gas to be isothermal with temperature T_e, and constant sound speed matched to the interface value:

$$c^2(r, z) \equiv c_e^2(r) = c^2(r, z_e) = \frac{\gamma R_g T_e(r)}{\mu}, \tag{41}$$

for $z > z_e$. Integrating the equation for hydrostatic equilibrium, we obtain the gas density:

$$\rho = \rho_m \left(1 - \Delta_e^2\right)^n \exp\left(-\frac{z^2 - \Delta_e^2 H^2}{2h_e^2}\right), \tag{42}$$

where

$$h_e^2 = \frac{c_e^2}{\gamma \Omega_{\rm K}^2} = \frac{c_m^2}{\gamma \Omega_{\rm K}^2}\left(1 - \Delta_e^2\right) = h^2\left(1 - \Delta_e^2\right). \tag{43}$$

4.3. *Location of the Photosphere*

To obtain z_e, we must solve the equation

$$\int_{z_e}^{\infty} \tilde{Z} \rho \kappa_e \, dz = \frac{2}{3}, \tag{44}$$

where $\kappa_e = \kappa_V (T_e/T_\star)^\beta$. Assuming that the dust is fully mixed with the gas (see eq. [1]) yields the required equation for Δ_e:

$$\left(1 - \Delta_e^2\right)^{n+\beta+1/2} \mathrm{erfc}\left(\frac{\theta \Delta_e}{\sqrt{2 - 2\Delta_e^2}}\right) \exp\left(\frac{\Delta_e^2 \theta^2}{2 - 2\Delta_e^2}\right) = \frac{2}{3}\sqrt{\frac{2}{\pi}} \frac{1}{\tilde{Z} \rho_m h \kappa_V} \left(\frac{T_m}{T_\star}\right)^{-\beta}. \tag{45}$$

This expression for Δ_e in terms of ρ_m and T_m at a given radius r seems rather complicated and requires in principle a numerical solution. However, there exist two limits in which a simple analytical solution exists. In the strongly opaque region (when the right-hand side of eq. [45] is very small) we expect z_e to be located high above the midplane and very close to H (so that $\Delta_e \simeq 1$). The nature of the polytropic/isothermal solution we are using implies that in this case we expect

$$1 - \Delta_e^2 = \varepsilon_e \ll 1, \quad \Delta_e \simeq 1 - \frac{\varepsilon_e}{2}. \tag{46}$$

Substituting this *Ansatz* into equation (45), and using the approximation given by equation (A2), we obtain

$$\varepsilon_e \simeq \left[\frac{(2/3)\theta^2 I(n)}{\tau_V^{\rm tot}}\right]^{1/(n+\beta+1)} \left(\frac{T_m}{T_\star}\right)^{-\beta/(n+\beta+1)}, \tag{47}$$

since in the limit where $z_e \simeq H$ the total surface density of the gas can be approximated by

$$\Sigma(r) = \int_{-\infty}^{\infty} \rho(r, z)\, dz \simeq \int_{-H}^{H} \rho(r, z)\, dz = 2\rho_m(r) H(r) I(n), \tag{48}$$

where

$$I(n) = \int_0^1 \left(1 - x^2\right)^n dx = \frac{1}{2} B\left(\frac{1}{2}, n + 1\right) \tag{49}$$

(B is a Beta function; see Gradshteyn & Rhyshik 1980, p. 343). From equation (47), we note that the approximation $\tau_V^{\rm tot} \gg 1$ is consistent with $\varepsilon_e \ll 1$. Note that this expression recovers the classical expression relating the midplane temperature to the effective temperature deduced from integrating the radiative flux and equating it with the total optical depth of the disk,

$$T_m^4 \propto \tau_V T_e^4, \tag{50}$$

valid in the limit of large optical depth. The proportionality constant depends on the set of assumptions made concerning the vertical distribution of the heating sources and the opacity law selected. Here we find that for $n = 2$,

$$T_m^4 = 0.84 \tau_V T_e^4. \tag{51}$$

In the alternative limit, the right-hand side of equation (45) approaches 1 (the disk is close to being optically thin), and we expect Δ_e to be very small, in which case an approximate solution can be obtained by linearizing equation (45),

$$\Delta_e \simeq \sqrt{\frac{\pi}{2}} \frac{1}{\theta}\left[1 - \frac{2/3}{\tau_V^{\rm tot}}\left(\frac{T_m}{T_\star}\right)^{-\beta}\right], \tag{52}$$

and using $\Sigma \simeq (2\pi)^{1/2} \rho_m h$.

The regimes of validity of the two approximations are illustrated in Figure 3. For the purpose of computations, we denote hereafter the "strongly opaque regime" as the region where we adopt the asymptotic approximation given by equation (47) and the "weakly opaque regime" as the region where we adopt equation (52) instead. Since we are not performing a rigorous matching between the two regions, we artificially patch them instead at the radius where the right-hand side of equation (45) reaches 0.1.

4.4. *Characteristics of the Superheated Dust Layer*

The calculation of the position of the superheated layer is similar to the isothermal case, but with a different vertical density distribution for the gas. As before, we use the stationary phase approximation assuming that the disk is flaring. In the weakly opaque limit, we retain the expressions derived in the optically thin case (namely, eqs. [21] and [24]), whereas in the strongly opaque limit (see the Appendix), we get

$$z_s \simeq H = \theta h, \tag{53}$$

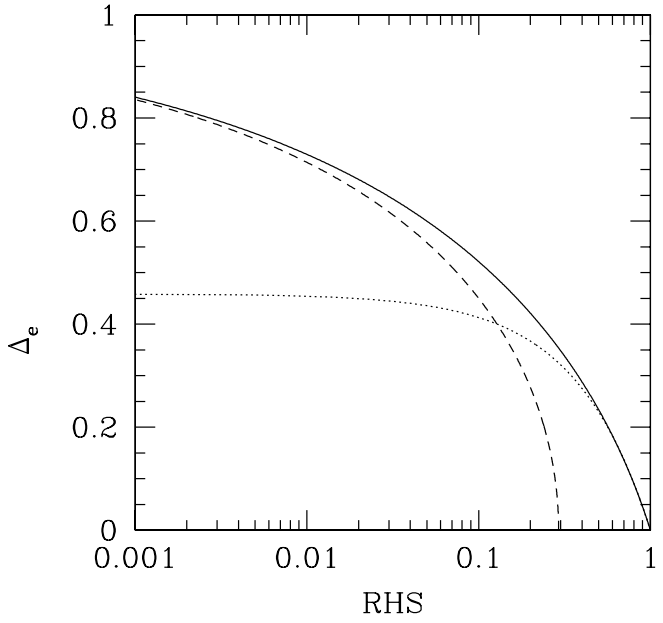

FIG. 3.—Comparison between the true solution to eq. (45) and the two asymptotic approximations. The x-axis represents the right-hand side of eq. (45). The solid line is the numerical solution, the dotted line is the approximation in the weakly opaque limit, while the dashed line is the approximation in the strongly opaque limit.

and as before

$$A_s = \frac{z_s}{h}\alpha \simeq \theta\alpha . \tag{54}$$

It is interesting to note at this point that in a completely isothermal model (as the one proposed by CG97), $C(r)$ increases monotonically with $\tau_V^{\rm tot}$ (eq. [21]). Here instead we show that $C(r)$ enters a different regime in the optically thick region and has a constant value set uniquely by the gas properties contained in θ (see eq. [38]).

4.5. *Radial Structure*

Weakly opaque region.—Now that we have all of the required information, we need to solve the total energy conservation equation. When the disk is nearly optically thin to its own radiation, the midplane temperature is very close to the photospheric temperature: the disk is nearly isothermal (typically, $\varepsilon_e \simeq 1$). In this case, we approximate, for simplicity, the total energy equation by

$$\frac{C}{2} r \frac{d}{dr}\left(\frac{h}{r}\right)\frac{R_\star^2}{r^2} = \left(\frac{T_e}{T_\star}\right)^4 \simeq \left(\frac{T_m}{T_\star}\right)^4 . \tag{55}$$

Integrating this equation for the disk scale height yields

$$\frac{\overline{h}}{1\ {\rm AU}} = \left(\frac{C}{7}\right)^{1/7}\left(\frac{\mu}{R_g}\frac{GM_\star}{R_\star T_\star}\right)^{-4/7}\left(\frac{R_\star}{1\ {\rm AU}}\right)^{-2/7}, \tag{56}$$

$$\frac{q+3}{2} = \frac{9}{7}, \tag{57}$$

so that $q = -3/7$ and for a steadily accreting disk $s = 15/14$. This result, once more, naturally recovers the radial power-law scaling found by CG97 since their work assumes that even optically thick disks are isothermal. Interestingly, we find that $\alpha = 2/7(h/r)$, which is notably smaller than the flaring angle in the nearby marginally opaque region (see eq. [29]). This difference indicates that the inclusion of the viscous dissipation reduces the flaring angle compared to a purely radiatively heated disk. This result is not surprising. The scale height of a standard disk is determined by the balance between the pinching force of gravity and the vertical pressure gradient, which is related to the local temperature. Thus, the flaring angle is related to the radial variation of the ratio of these two quantities. In the case of a radially isothermal disk, the flaring angle is maximal since gravity quickly decreases outward. In the case of radiatively heated disks, the addition of a negative temperature gradient implies that temperature increases inward and reduces the flaring. Finally, the additional contribution from viscous heating to the midplane temperature further reduces the flaring.

What is more counterintuitive is that the inclusion of viscous dissipation can, in some regions, reduce the photospheric temperature of a disk compared to a model in which it is not taken into account: *additional heating does not necessarily mean apparently hotter disks*. This happens in regions where viscous heating is only important in maintaining a warmer midplane but does not contribute much to the overall energy budget. In this case, the reduced flaring angle implies a reduced intercepted stellar flux and therefore a cooler photospheric temperature.

Strongly opaque regions.—In what follows, we show how our formalism is able to extend the model of CG97 to nonisothermal, strongly opaque disks. In this new limit, we use the fact that $T_e = \varepsilon_e T_m$ with equation (47). After a few manipulations we get

$$\begin{aligned}\frac{\overline{h}}{1\ {\rm AU}} = &\left(\frac{2n+2-4s-2\beta}{7n+7-\beta}\frac{\theta}{2}\right)^{(n+\beta+1)/(7n-\beta+7)} \\ &\times\left(\frac{\mu}{R_g}\frac{GM_\star}{R_\star T_\star}\right)^{-(4n+4)/(7n+7-\beta)} \\ &\times\left(\frac{4}{3}\frac{\theta^2 I(n)}{\tilde{Z}\overline{\Sigma}\kappa_V}\right)^{-4/(7n+7-\beta)} \\ &\times\left(\frac{R_\star}{1\ {\rm AU}}\right)^{-(2n+2-2\beta)/(7n+7-\beta)},\end{aligned} \tag{58}$$

$$\frac{q+3}{2} = \frac{9n+9-3\beta-4s}{7n+7-\beta}. \tag{59}$$

In the case of a steadily accreting disk, we combine these equations with equation (14) to obtain

$$\begin{aligned}\frac{\overline{h}}{1\ {\rm AU}} = &\left(\frac{2n-2\beta}{7n+15-\beta}\frac{\theta}{2}\right)^{(n+\beta+1)/(7n-\beta+15)} \\ &\times\left(\frac{\mu}{R_g}\frac{GM_\star}{R_\star T_\star}\right)^{-(4n+4)/(7n+15-\beta)} \\ &\times\left[\frac{4\pi\alpha_t\sqrt{\gamma GM_\star R_\star}\theta^2 I(n)}{\tilde{Z}\kappa_V\dot{M}}\right]^{-4/(7n+15-\beta)} \\ &\times\left(\frac{R_\star}{1\ {\rm AU}}\right)^{-(2n-2\beta)/(7n-\beta+15)},\end{aligned} \tag{60}$$

$$s = \frac{15n+15-9\beta}{2(7n+15-\beta)}. \tag{61}$$

With $\beta = 1$ and $n = 2$, we obtain $s \simeq 0.65$ and $q \simeq -0.85$, which confirms again that the disk is flaring. However, we note that in this case the flaring is even weaker ($\alpha \simeq 0.1h/r$), and the disk surface is very nearly flat. Again, this geometry has very important consequences for the overall inner disk temperature,

since a much lower fraction of the stellar luminosity is intercepted than in a model in which the disk is assumed to be isothermal (see the previous case).

Viscously heated disks.—Finally, if the dominant contribution to the heating of the disk arises from viscous dissipation instead of stellar irradiation, manipulations of the total energy equation (7) imply that

$$T_e = \left(\frac{3GM_\star \dot{M}}{8\pi\sigma}\right)^{1/4} r^{-3/4}, \tag{62}$$

which can then be used to deduce h, as usual:

$$\begin{aligned}\frac{\overline{h}}{1\ \mathrm{AU}} &= \left(\frac{3}{2}\frac{L_{\mathrm{acc}}}{L_\star}\right)^{(n+\beta+1)/(8n+8)} \left[\frac{4\theta^2 I(n)}{3\kappa_V \overline{\Sigma}\tilde{Z}}\right]^{-1/(2n+2)} \\ &\quad \times \left(\frac{\mu GM_\star}{R_g R_\star T_\star}\right)^{-1/2} \left(\frac{R_\star}{1\ \mathrm{AU}}\right)^{(3\beta-n-1)/(8n+8)}, \\ \frac{q+3}{2} &= \frac{9n-3\beta+9-4s}{8(n+1)},\end{aligned} \tag{63}$$

where we define here $L_{\mathrm{acc}} = GM_\star \dot{M}/R_\star$. In the case of steady accretion, we can reduce this further to yield

$$\begin{aligned}\frac{\overline{h}}{1\ \mathrm{AU}} &= \left(\frac{3}{2}\frac{L_{\mathrm{acc}}}{L_\star}\right)^{(n+\beta+1)/(8n+16)} \\ &\quad \times \left[\frac{4\theta^2 I(n)}{\kappa_V \tilde{Z}}\frac{\pi\alpha_t}{\dot{M}}\sqrt{\gamma GM_\star R_\star}\right]^{-1/(2n+4)} \\ &\quad \times \left(\frac{\mu}{R_g}\frac{GM_\star}{R_\star T_\star}\right)^{-(n+1)/(2n+4)} \\ &\quad \times \left(\frac{R_\star}{1\ \mathrm{AU}}\right)^{(3\beta-n+1)/(8n+16)}, \\ \frac{q+3}{2} &= \frac{9n-3\beta+15}{8n+16}.\end{aligned} \tag{64}$$

With the adopted fiducial values for n and β, we find that the viscously heated regime is the only one that is not flaring: indeed, in this case $q = -1.125$ and $s = 0.375$. However, flaring is not self-consistently required toward the determination of the disk structure in this region, so the formula given above is in fact valid. One may wonder, however, whether the viscously heated regions could shadow the innermost radiatively heated regions, as proposed by Dullemond & Dominik (2004) for Herbig Ae/Be (HAeBe) stars. We do not believe that this is the case for classical T Tauri stars: it should first be noted that the disk is still very nearly flat (q is very close to -1), and secondly that the radial extent of the viscously heated region is small (which is not the case for HAeBe stars).

5. POSITION OF THE TRANSITION RADII

In this section we derive analytical expressions for the position for the transition radii across the various regions for the specific case where the disk undergoes steady state accretion. For simplicity we give the formula for the specific case where $\beta = 1$ and under the assumption of steady state accretion, although they can also be easily derived in the general case. In practice, the transition radii are most easily computed numerically.

5.1. *Transition from Optically Thin to Marginally Opaque*

This transition occurs when $\tau^s_{\mathrm{tot}} = 1$, or equivalently when

$$\frac{\dot{M} r^{-s}}{3\pi\alpha_t \sqrt{\gamma GM_\star}\overline{h}^2}\frac{\kappa_V \tilde{Z}}{2}\left(\frac{R_\star^2}{r^2}\right)^{1/5} = 1, \tag{65}$$

where s and $\overline{h}$ are derived from equation (26). Solving for the transition radius $r^{t\to m}$ yields

$$\begin{aligned}r^{t\to m}_{\mathrm{AU}} &= \left(\frac{\tilde{Z}\kappa_V}{2}\frac{\dot{M}}{3\pi\alpha_t\sqrt{\gamma GM_\star R_\star}}\right)^{90/133} \\ &\quad \times \left[\frac{1}{C}\frac{45}{13}\left(\frac{\mu}{R_g}\frac{GM_\star}{R_\star T_\star}\right)^5\right]^{20/133}\frac{R_\star}{1\ \mathrm{AU}}.\end{aligned} \tag{66}$$

We see that, as expected, this transition moves inward as the disks evolve and their mass accretion rate decreases.

5.2. *Transition from Marginally Opaque to Optically Thick*

This transition occurs when $\tau^m_{\mathrm{tot}} = \tilde{Z}\Sigma\kappa_m/2$ reaches $\frac{2}{3}$, or equivalently, when the right-hand side of equation (45) reaches unity. In a steadily accreting disk, with $\beta = 1$, the right-hand side of equation (45) reduces to

$$\frac{2}{3}\sqrt{\frac{2}{\pi}}\frac{1}{\tilde{Z}\rho_m h\kappa_V}\left(\frac{T_m}{T_\star}\right)^{-1} \simeq \frac{2\sqrt{2\pi\gamma}K\alpha_t}{\tilde{Z}\kappa_V\dot{M}}\frac{R_g T_\star}{\mu\Omega_{\mathrm{K}}}, \tag{67}$$

where K varies slowly between $(2\pi)^{1/2}$ (in the nearly optically thin case) and $2I(n)\theta$ (in the very optically thick case). This implies that for given accretion parameters $\dot{M}$ and α_t and given stellar parameters $T_\star$ and $M_\star$, the transition radius at which the disk changes from optically thick to optically thin to its own radiation is entirely determined and equal to

$$r^{m\to o}_{\mathrm{AU}} = \left(\frac{\tilde{Z}\kappa_V}{2}\frac{\dot{M}}{2\pi\alpha_t}\sqrt{\frac{GM_\star}{\gamma R_\star^3}}\frac{\mu}{R_g T_\star}\right)^{2/3}\frac{R_\star}{1\ \mathrm{AU}}. \tag{68}$$

Again, as expected, this transition moves inward as the disks evolve and their mass accretion rate decreases. It is interesting to note, however, that to a good degree of approximation both $r_{t\to m}$ and $r_{m\to o}$ are proportional to $\dot{M}^{2/3}$, which implies that the ratio $r^{t\to m}/r^{m\to o}$ is independent of mass accretion rate.

5.3. *Position of the Snow Line*

The outer edge of the snow line is located where T_m first reaches 160 K. This transition can happen either in the optically thin region or in the optically thick region. In both cases, its position is given by the equation

$$r^{\mathrm{snow}}_{\mathrm{AU}} = \left[\frac{160R_g}{\overline{h}^2\mu}\frac{(1\ \mathrm{AU})^3}{GM_\star}\right]^{1/q}, \tag{69}$$

where $\overline{h}$ and q are region dependent. In the optically thick case (for $\beta = 1$, and n and θ given by eq. [38]), we find that

$$r^{\mathrm{snow}}_{\mathrm{AU}} \propto \dot{M}^{1/3} \tag{70}$$

so the snow line moves inward as the mass accretion rate decreases. Since this migration rate is slower than the rate at which

the optically thin region expands, there must be a point where the snow line becomes optically thin. When this happens, its location moves outward again to a radius that is a function only of the stellar parameters (with a weak dependence on the disk structure through C). When $\beta = 1$,

$$r_{\rm AU}^{\rm snow} = \left(\frac{160 R_g}{T_\star}\right)^{-45/19} \left(\frac{45}{13C}\right)^{-10/19} \times \left(\frac{\mu}{R_g}\frac{GM_\star}{R_\star T_\star}\right)^{-5/19} \frac{R_\star}{1\ {\rm AU}}. \quad (71)$$

The smallest possible radius attained by the snow line in the course of the disk evolution can be estimated simply by finding the position of the snow line while it is located in the weakly opaque region. We find that

$$\min\left(r_{\rm AU}^{\rm snow}\right) \simeq 0.6\ {\rm AU} \left(\frac{L_\star}{L_\odot}\right)^{2/3} \left(\frac{M_\star}{M_\odot}\right)^{-1/3}. \quad (72)$$

This can be considered as the minimum radius at which a significant amount of vapor-phase water can be found in protoplanetary disks in the course of their evolution. Most importantly, note that this value is independent of the value of κ_V selected and of the nature of the polytropic solution selected: it is uniquely determined by the properties of the central star. However, the value of $\dot{M}$ for which this minimal position is achieved does depend on these disk properties.

In § 7 we discuss in more detail the evolution of the position of the snow line as the disk evolves and its consequences for planet formation.

5.4. *Transition from Radiatively Heated to Viscously Heated*

This transition occurs when viscous heating and radiative heating are of the same order of magnitude. In a steady state accretion approximation, we deduce the transition radius from equating

$$\frac{3}{4\pi}\dot{M}\Omega_{\rm K}^2 = 2\frac{A_s}{2}\frac{L_\star}{4\pi r^2} \quad (73)$$

to be

$$r_{\rm AU}^{\rm visc} = \left(\frac{3L_{\rm acc}}{SL_\star}\frac{R_\star}{\overline{h}}\frac{2}{q+1}\right)^{2/(q+3)}, \quad (74)$$

where the constant S is either θ, if the transition radius occurs in strongly opaque regions, or C, if it is located in optically thin, marginally, or weakly opaque regions. The exact values of $\overline{h}$ and q also depend on the radial region considered.

6. EXAMPLES OF STAR/DISK SYSTEMS

6.1. *Examples of Protostellar Disks around a Weak-Line T Tauri Star*

We now apply our model to dusty disks around T Tauri stars. We defer to later publications the discussion disks around the more massive HAeBe stars and around the low-mass brown dwarfs. Direct comparison between our model and the predictions of the CG97 model is presented in the discussion section.

For the purpose of computing the structure of the disk, we select the following values for the global stellar and disk properties (except when explicitly mentioned):

$$L_\star = 1\ L_\odot, \quad M_\star = 1\ M_\odot, \quad R_\star = 1\ R_\odot,$$
$$\tilde{Z} = 2, \text{ equivalent to } Z = 0.02,$$
$$\alpha_t = 10^{-3},$$
$$\mu = 2.4, \quad \gamma = 1.4, \quad (75)$$
$$n = 2,$$
$$\kappa_V = 1\ {\rm cm^2\ g^{-1}}, \quad \beta = 1,$$
$$C = 4. \quad (76)$$

We also vary the mass accretion rate from $\dot{M} = 10^{-8}$ to $10^{-10}\ M_\odot\ {\rm yr}^{-1}$, to cover a range of gas accretion rates from observed values for classical T Tauri stars (Hartmann 2001) down to low values presumably corresponding to a protostellar-debris disk transition. The results are shown in Figure 4.

Comparisons of the solutions for a particular value of $\dot{M}$ for two values of the polytropic index n and the grain opacity κ_V are shown in Figure 5. We note that while the choice of the polytropic index only has a small effect on the radial structure of the disk, the choice of the opacity naturally influences the transition between the optically thick and optically thin regions of the disk.

For each accretion rate, three figures are shown: (1) the various relevant surfaces [$h(r)$, $z_s(r)$, and $z_e(r)$], (2) the relevant temperature profiles [$T_m(r)$, $T_s(r)$, and $T_e(r)$], and (3) the surface density profile. In each case, the superheated grain position and temperature are shown as a dotted line. Note that T_s depends only on the nature of the central star: the profiles obtained in all three values of $\dot{M}$ for the particular T Tauri star chosen are identical. The position and temperature of the photosphere are shown as a solid line. The midplane temperature and its associated disk scale height h are shown as long-dashed lines.

The three regions (from right to left, optically thin, marginally optically thin, and optically thick, with the latter subdivided into weakly opaque, strongly opaque, and viscously heated regions) are clearly visible in each figure. The transition radii from optically thin to marginally opaque and from marginal to optically thick are genuine physical transitions and are marked by vertical dashed lines. We observe that the transition from an optically thin to a marginal region is associated with a fairly continuous temperature profile, while that from marginal to optically thick has an important temperature discontinuity. Note that in a real disk the temperature "jump" would be more diffuse (as a result of radial thermal and viscous diffusion processes unaccounted for in our 1+1D model) and could span a radial extent of up to 1 scale height. The artificial transitions and associated discontinuities observed in the opaque region (from left to right), between radiatively heated and viscously heated regions and between the weakly opaque and strongly opaque regions, are mathematical artifacts of our crude patching procedure between various asymptotic approximations (in the former case for the dominant heating mechanism, and in the latter for eq. [45]); they are represented by dotted vertical lines. One can estimate the true profile by smoothly matching one region to the next across these dotted lines by eye or, should one desire a more accurate solution, actually solve the problem numerically.

Finally, the vertical solid line represents the snow line for the midplane temperature. Across this line, the equations presented here are only qualitatively valid, since we neglect all effects associated with the sublimation of the ices. We describe in detail a

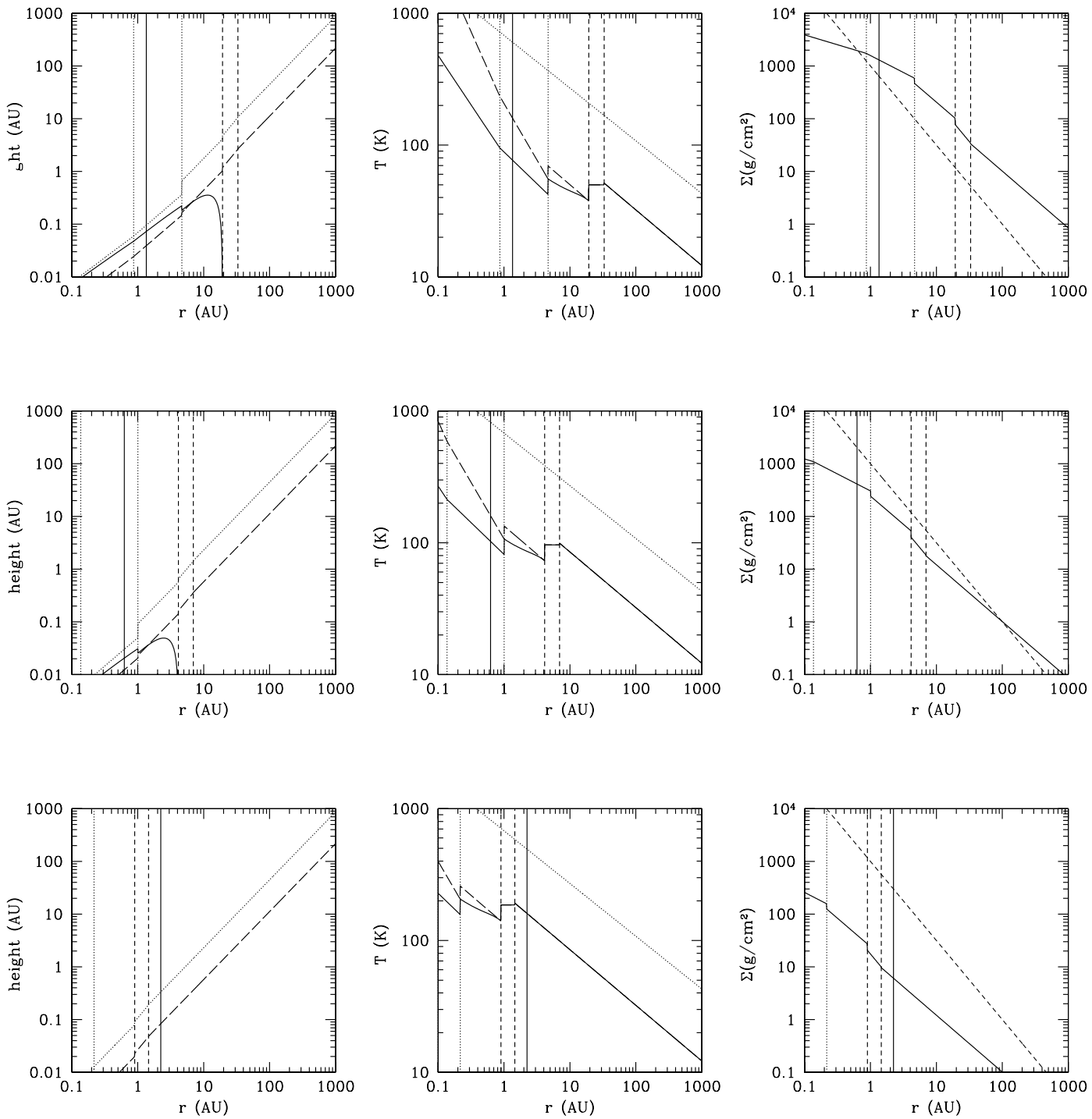

FIG. 4.— Model prediction for a T Tauri star disk with accretion rates (*top to bottom*) of $\dot{M} = 10^{-8}$, 10^{-9}, and $10^{-10}\,M_{\odot}\ \mathrm{yr}^{-1}$. The left panels show the various important surfaces and heights, the middle panels show the relevant temperature profiles, and the right panels show the surface density profiles. On the left, the dotted line marks the position of the superheated layer $z_s(r)$, the long-dashed line marks the disk temperature scale height $h(r)$, and the solid line marks the position of the photosphere $z_e(r)$. In the middle, the dotted line marks the temperature of the superheated grains T_s, the long-dashed line marks the temperature of the midplane T_m, and the solid line marks the effective temperature T_e. On the right, the solid line marks our model prediction for $\Sigma(r)$, while the thick dashed line is the standard MSN profile $\Sigma_{\mathrm{MSN}} = 1000 r_{\mathrm{AU}}^{-3/2}\ \mathrm{g\ cm}^{-2}$. In all diagrams, the snow line for the midplane temperature appears as a vertical solid line. The vertical dashed lines (when present, from left to right) denote the physical transitions from the optically thick to the marginally optically opaque region, and then to the optically thin region. The vertical dotted lines mark the position of the artificial transitions between asymptotic regimes: near the central star (and in these diagrams, on the left of the snow line when present), the transition from viscously heated to radiatively heated, and near the marginally opaque region, the transition from the largely opaque region to the weakly opaque regions.

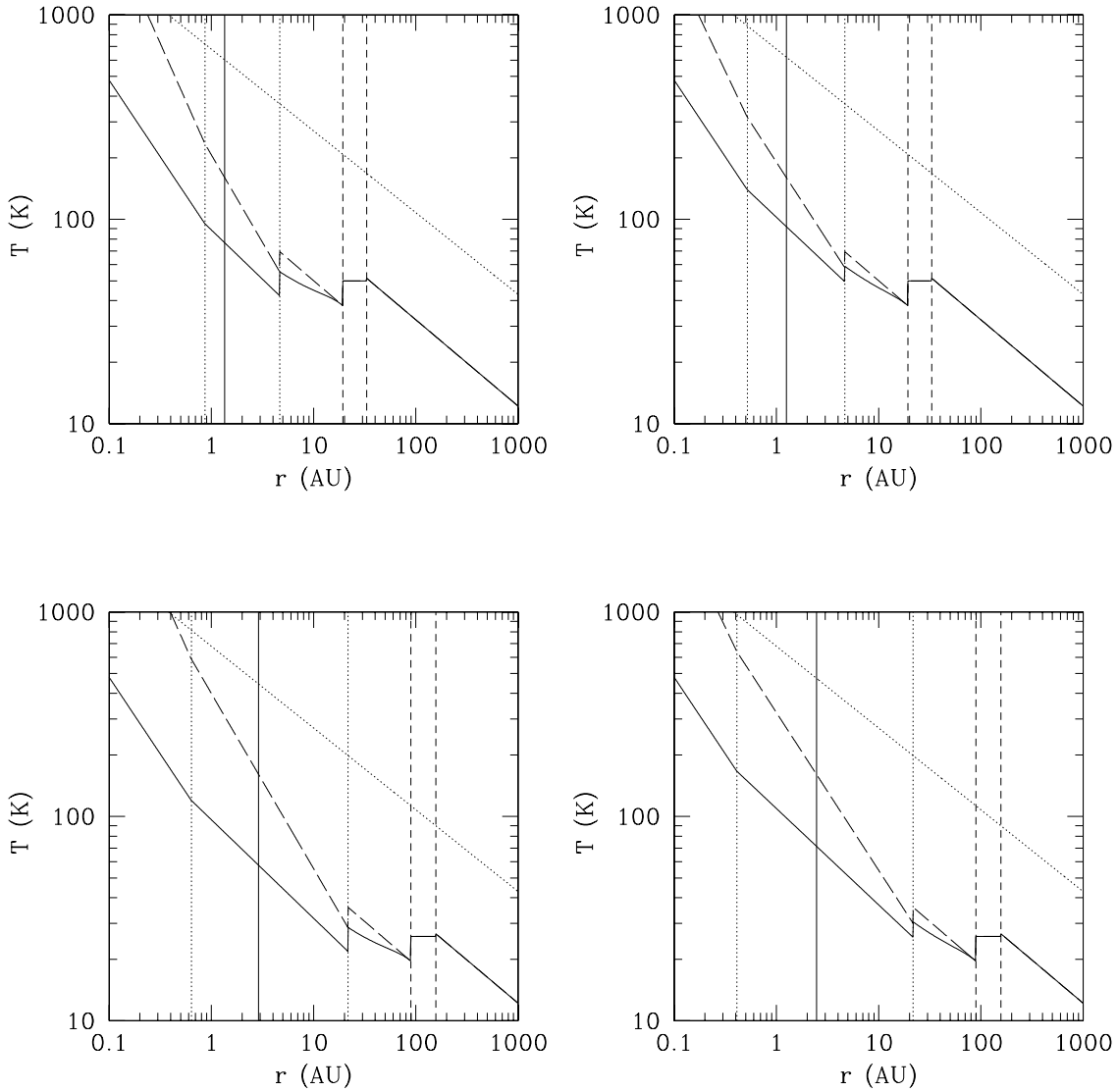

FIG. 5.—Comparison of the model predictions for the temperature profiles of a disk with $\dot{M} = 10^{-8}\, M_{\odot}\ \mathrm{yr}^{-1}$ around a solar-type star, for two values of κ_V (from top to bottom $\kappa_V = 1$ and 10 $\mathrm{cm}^2\ \mathrm{g}^{-1}$) and two values of the polytropic index n (from left to right $n = 2$ and 3). The four panels are otherwise generated using the same conventions as in Fig. 4. Note that the choice of the polytropic index n has only a small qualitative influence on the solution in the optically thick regions of the disk (and naturally no influence on the optically thin regions), while the opacity κ_V influences strongly the position of the transition between optically thin and optically thick regions of the disk.

new snow line model in a following paper. Note that the temperature of the superheated grains reaches 160 K at a far greater radius than the marked (midplane) snow line. The sublimation of the icy particles in the superheated layer results in a drop in $\tilde{Z}$ above z_s, but as shown in equation (21), this would only have a small effect on the value of $C(r)$. Hence, in what follows we ignore the effect of the successive sublimation lines on the structure of the superheated layer.

Note that since the outer edge of the disk depends on a number of potentially important factors (initial radius, self-shadowing in the very optically thin case, total mass, thin-disk approximation, etc.), we have not marked it on the figures presented. The reader should also bear in mind that the model has less predictive power in regions much beyond 100 AU, where the assumptions inherent to steady state accretion are no longer satisfied; in these regions, the problem is best solved as an initial value problem.

Several notable qualitative features can be readily seen from these T Tauri star models and are also found in disks with a wide range of accretion rates, around stars with a wide range of stellar types.

First, we observe the presence of a wide, radially isothermal region (corresponding to the marginally opaque region). Although the isothermal nature of this section of the disk was already inferred by CG97, we find that it also has the remarkable property of being notably hotter than the region immediately within, so that *the overall photospheric temperature profile is not a monotonically decreasing function of radius*. The hotter temperature is a result of the larger flaring angle of this region compared to the one within, implying that a larger fraction of the stellar flux is absorbed locally. The presence of a "hot ring" could have very interesting consequences, both from an observational point of view and from the point of view of the dynamics of dust grains in the disk. This is discussed in detail in § 7.

Second, although a more rigorous snow line model will be needed for more accurate quantitative discussions, it is already apparent in the models presented that the radial extent of the

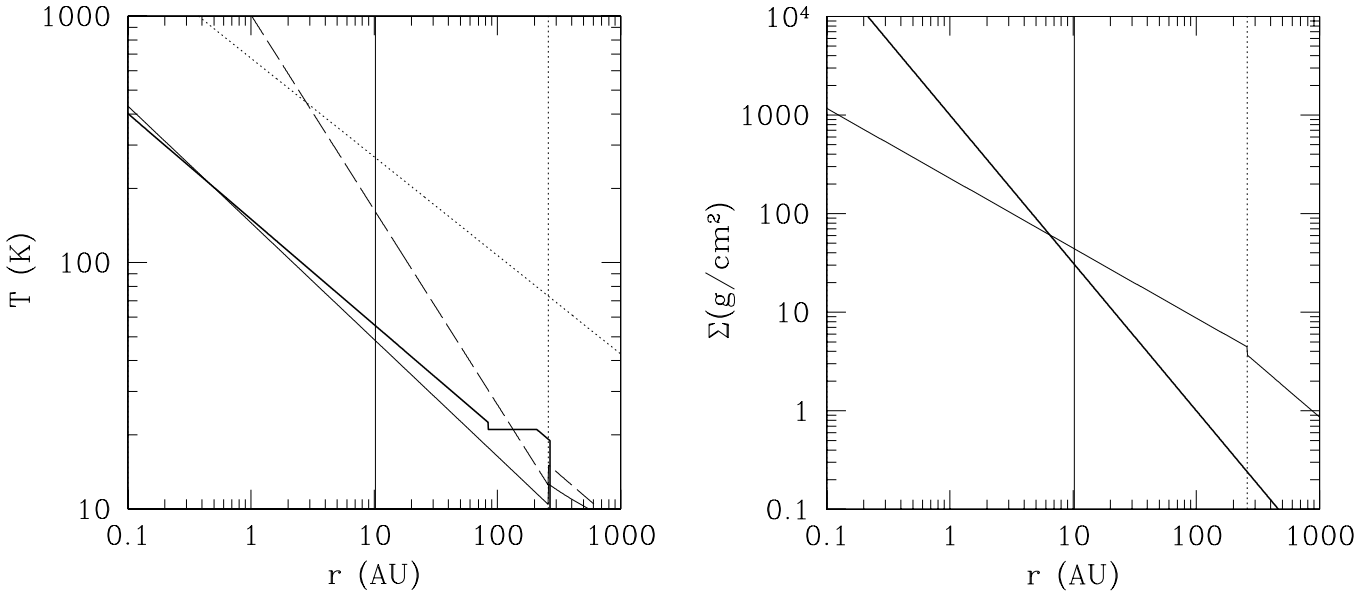

FIG. 6.—Direct comparison between our model predictions (*thin lines*; line style coding as in Fig. 4) and the CG97 model predictions (*thick line*) for the temperature and surface density in a disk around typical T Tauri stars with mass 0.5 $M_\odot$, radius 2.5 $R_\odot$, and effective temperature 4000 K. Note in particular the lower effective temperature of our model, the much higher midplane temperature, and the higher surface density in the outer regions. The predictions for the temperature of the superheated grains are naturally identical.

snow line can be considerable when it lies within the optically thick region. By radial extent, we imply the region between the radius at which the midplane temperature becomes equal to the ice sublimation temperature and the radius at which the photospheric temperature reaches the same value. For example, our results indicate that for a standard accretion rate of $10^{-8}\ M_\odot\ \mathrm{yr}^{-1}$, the snow line extends from 0.4 (where $T_e = 160$ K) to 1.35 AU (where $T_m = 160$ K). We also note that its extent increases with mass accretion rate (see also Fig. 7). On the other hand, for low mass accretion rates (for a 1 $M_\odot$, 1 $L_\odot$ T Tauri star when $\dot{M} < 10^{-10}\ M_\odot\ \mathrm{yr}^{-1}$) we find that the snow line is located in the optically thin region, with entirely different physical and dynamical characteristics. The consequence of the transition from an optically thick to an optically thin snow line will be discussed in more detail in a forthcoming paper.

Third, we note that the predicted overall surface density profile is notably shallower than an MSN model. Only in the marginally opaque region do we reproduce the standard MSN radial power-law scaling. This is discussed in more detail in § 7.

7. DISCUSSION OF THE RESULTS AND OBSERVATIONAL PROSPECTS

Our new disk model is based on that proposed by CG97, but it contains two significant additions. In our analysis, a polytropic assumption for the disk in optically thick regions enables us to study the largely nonisothermal structure of typical inner disks, while retaining the analytical nature of the mathematical solutions. We have also incorporated the contribution to heating due to viscous dissipation, which necessarily accompanies mass accretion. In addition, unlike CG97, we do not assume an MSN surface density profile. We can therefore calculate self-consistently all disk quantities as a function of radius assuming steady state accretion or, as we shall consider in a future investigation, solve numerically for the temporal evolution of the disk as an initial value problem, using the mass accretion rates derived in the model.

In this section we begin by a direct comparison of our model predictions with those of CG97 using their chosen fiducial T Tauri star characteristics. Then, we critically discuss the model assumptions and finally the model predictions in the light of recent observational and theoretical advances.

7.1. *Comparison with the Chiang & Goldreich Model*

We compare our model predictions for the temperature profile in a protostellar disk around a 0.5 $M_\odot$, 2.5 $R_\odot$ T Tauri star to the formula given by CG97 based on their isothermal model. A straightforward comparison is impossible since the mass accretion rate in their model varies between about 5×10^{-7} and about $2 \times 10^{-8}\ M_\odot\ \mathrm{yr}^{-1}$ (assuming the same value of α_t in both models), as a result of their assumed surface density profile. On the other hand, we need to fix $\dot{M}$, so we choose a fiducial value of $\dot{M} = 10^{-8}\ M_\odot\ \mathrm{yr}^{-1}$ for the purpose of the comparison. In addition, for this simulation only we change the opacity κ_V to the value of 400 cm^2 g^{-1} used by CG97. The results are shown in Figure 6.

We note first that regardless of the inherent difficulty in comparing models with different assumptions, the predictions for the photospheric temperatures do, at a first glance, match fairly well. This agreement is expected since the only difference in the total energy budget in the optically thick, radiatively heated regions of the disk arises from slightly different predicted flaring angles in the two approaches. However, beyond this overall match, we note several points of discrepancy.

First, the photospheric temperature in the optically thick inner nebula in our model is in fact systematically lower than theirs by 10%–20%, except very near the central star. This difference solely arises from the lower flaring angle predicted when heating is taken into account in the disk midplane.

Second, the position of the transition between optically thick and optically thin regions of the disk is closer to the central star in their model than in ours. This mismatch is caused by our largely different prediction for the surface density profile of the disk, which implies that the outer regions have higher overall mass content (and optical depth) than in a standard MSN model for the mass accretion rate considered.

Finally, note that their isothermal model predicts a snow line located around 1 AU, while taking into account the nonisothermal nature of the optically thick region implies that the snow line extends as far out as 10 AU for this particular T Tauri star. Indeed, at 1 AU, for instance, our midplane temperature is $\sim 10^3$ K and exceeds the photospheric temperature by a factor of 5. Neglecting this effect can lead to a gross miscalculation of the position of the snow line.

7.2. *The Validity of the Model Assumptions*

The three major assumptions of the proposed model are the following: viscous dissipation is modeled by an ad hoc α-prescription, the disk stratification is modeled as a polytrope in optically thick regions, and finally the dust grains are assumed to be uniformly mixed with the gas at all heights and radii.

Turbulent viscous dissipation affects the disk in two ways: it promotes the outward transfer of angular momentum, enabling gas accretion onto the central star, and generates heat preferentially in the midplane of the disk. For modest accretion rates, the viscous contribution to the total energy budget of the disk at any particular radius is significant only well within the snow line. However, it does play a role in driving a small temperature gradient between the midplane and the photosphere in optically thick regions well outside of the snow line. By modeling the turbulent viscous dissipation using an α-prescription, we implicitly assume that the mechanism driving turbulence is robust and independent of position within the disk.

While observations ubiquitously suggest that accretion is an ongoing process in protostellar disks (Hartmann 2001) and that it must be approximately quasi-steady (otherwise, strong accumulation of matter near specific locations in the disk would be systematically observed), the origin of turbulence still remains largely unclear. Turbulent mixing cannot be of convective nature only, since heating of the surface layers may suppress convection (Watanabe et al. 1990). Mixing by a magnetorotational instability (MRI; Balbus & Hawley 1991) is difficult to sustain in regions where the ionization fraction of the gas is too low (the dead zones). Although surface layers of the disk are always potentially subject to the MRI since they are exposed to a significant ionizing flux from both cosmic rays and the central star (Gammie 1996), it is not clear that turbulent motions driven high above the disk are strong enough to sustain a high α-value all the way down to the disk midplane. Finally, turbulent mixing by a subcritical instability of the background Keplerian shear has also been proposed (Richard & Zahn 1999; Dubrulle et al. 2005), as well as shearing instabilities in the midplane layer caused by the sedimentation of the dust particles (Goldreich & Ward 1973; Weidenschilling & Cuzzi 1993; Garaud & Lin 2004; Gomez & Ostriker 2005), but while the former has not yet been formally proven to exist, the typical growth rates of the latter may be too long compared with the dynamical timescale to be effective in providing a reliable source of angular momentum mixing.

To complicate matters, it is likely that the intrinsic disk stratification (both radially and across the midplane) may result in largely nonuniform turbulent transport properties. Thus, we recognize that the α-prescription is merely an ad hoc assumption, necessary to our simplified treatment, and now discuss to which extent the results we obtain are model dependent.

In our model, the α-prescription is used to calculate the surface density profile of disks under the assumption of steady state accretion. Consequently, if α varies significantly with radius, the radial profiles obtained in the steady state accretion assumption must be modified accordingly, and the radial scaling laws obtained should be revised entirely.

The generation of heat by viscous dissipation is, on the other hand, subtly disguised in our model by the assumption of a polytropic stratification for the gas/dust mixture. Thus, the model is indirectly dependent on α through the polytropic index assumed.

Finally, the last questionable assumption of the model involves the fully mixed nature of the dust grains with the gas. Grains are fully suspended in the gas only when their stopping time is much longer than the turnover time of the turbulent eddies (which are no more than 1 order of magnitude larger than the orbital time). For the smallest grains (typically 0.1 μm), which are responsible for most of the absorption of the stellar light within the superheated layer, this approximation is largely satisfactory at all radii. Thus, we do not expect the position and structure of the superheated layer to be affected by this simplified approximation: significant sedimentation of larger grains (millimeter size) will leave the superheated layer unaffected. On the other hand, the disappearance of the smallest grains resulting from the *overall* growth may result in a change in $C(r) = z_s/h$ by a factor of order unity. This possibility should be taken into account self-consistently in future models. With respect to the midplane and radial structure, grain growth results in a change in κ_V and β, which will affect the radial temperature distribution (and therefore the spectral slope) in all regions of the disk. Sedimentation does not affect the reprocessing of light in the optically thin regions but may have a detectable effect on the position of the photosphere (and therefore the radial profile) in the optically thin regions.

7.3. *Discussion of the Results and Their Observational Implications*

Disk geometry.—As in CG97, we find that the stellar radiation is primarily absorbed by a flaring layer ($\alpha > 0$) of superheated grains in the radiatively heated regions, including the newly studied case of optically thick, nonisothermal disks. Regions where viscous dissipation is the principal source of energy are, on the other hand, found to be nonflaring ($\alpha < 0$) although their overall geometry is very close to flat.

From the central regions to the outer regions of the disk we find that the flaring angle gradually increases outward. The viscously heated, and radiatively heated, strongly opaque regions of the disk are close to a flat geometry ($\alpha = 0$), with the temperature index q increasing from -1.125 to -0.85 (corresponding to $\alpha \simeq -0.0625h/r$ and $\alpha \simeq 0.075h/r$, respectively). Thus, we note that a flat disk geometry does not necessarily imply any grain sedimentation, and it can also straightforwardly be reproduced by an appropriately modeled optically thick disk.

The marginally opaque transition region (from optically thick to optically thin disks) is accompanied by a very sharp, local increase in the flaring angle with $\alpha = 0.5h/r$. This transition is therefore accompanied by a sharp local increase in the temperature, reaching values up to 40% larger than in the optically thick region immediately within.

Self-consistent calculations of the height of the superheated layer in the optically thin regions show that the flaring geometry persists all the way out to several hundred AU, albeit with a slightly smaller flaring angle ($\alpha \simeq 0.3h/r$).

Self-shadowing of the outermost regions may occur, as discussed earlier, when α exceeds a fraction of the total visual optical depth, unless other mechanisms truncating the disk occur first. This sharp cutoff in the reprocessed radiation could appear as an outer edge of the disk.

Disk SEDs and surface density distribution.—The mid-IR and far-IR photons are emitted both by grains at the photosphere of the inner opaque regions where $T_e < 200$ K and by the superheated

grains with $T_\star < 200$ K at much larger radii. Around classical T Tauri stars where $\dot{M} \sim 10^{-7}\ M_\odot\ \mathrm{yr}^{-1}$, the radii where T_e and $T_\star$ decrease below 200 K are 0.7 and 30 AU, respectively. Around weak-line T Tauri stars with $\dot{M} \sim 10^{-9}\ M_\odot\ \mathrm{yr}^{-1}$ the radii where they fall below 200 K are 0.07 and 30 AU, respectively. Although the area filling factor $A_s \sim \alpha$ of the superheated grains with $T_\star < 200$ K is well below unity, their total emitting area is much larger than the opaque inner region with $T_e < 200$ K. Consequently, the superheated grains contribute to a large fraction of the mid-IR and far-IR radiation and the SED in this wavelength range is essentially flat (CG97).

The magnitude of T_e of the opaque regions is generally too high for the emerging photons to contribute significantly to the submillimeter radiation. These photons are emitted by much cooler and much larger (millimeter to centimeter size) grains near the midplane of marginally transparent and optically thin regions in the outer disk. At very large disk radii, the superheated grains also contribute to these long wave radiations.

A robust feature of our model is the prediction of an overall disk surface density much shallower than the standard MSN; this prediction is associated with the assumption of steady state accretion. More precisely, we find that the opaque inner disk regions satisfy roughly $\Sigma \propto r^{-0.4}$ and $r^{-0.7}$ in the viscously and radiatively heated regions, respectively. The marginally opaque disk regions, however, are radially isothermal, which implies a surface density profile varying as the MSN profile (Hayashi et al. 1985) under the steady state accretion approximation. This is particularly interesting since these intermediate regions can have a large radial extent (between 100–200 AU and 4–7 AU, respectively, as $\dot{M}$ decreases from 10^{-7} to $10^{-9}\ M_\odot\ \mathrm{yr}^{-1}$). Finally, in the optically thin regions we find $\Sigma \propto r^{-1.08}$. Around some T Tauri stars, the outer regions have been resolved by millimeter interferometer observations. Our prediction on the surface density distribution in this region is very similar to that inferred from the millimeter maps of resolved protostellar disks around T Tauri stars (Mundy et al. 2000; Looney et al. 2003). The disk mass determination based on the assumption that these regions are optically thin (Beckwith & Sargent 1991) is fully justified.

Snow line position, structure, and history.—As seen in Figure 4, the snow line around 1 $M_\odot$ classical T Tauri stars shrinks from a few to about 0.6 AU as $\dot{M}$ decreases from 10^{-7} to $10^{-10}\ M_\odot\ \mathrm{yr}^{-1}$, then reexpands to slightly over 2.2 AU. This interesting nonmonotonous variation of the snow line position with mass accretion rate (and therefore with time) is illustrated in Figure 7.

For relatively high values of the mass accretion rate, we confirm that the snow line is located in the strongly opaque region and therefore has a significant radial extent. For $\dot{M} \sim 2 \times 10^{-7}\ M_\odot\ \mathrm{yr}^{-1}$ the snow line is located near the present-day radius of Jupiter; it may have been critical in promoting the emergence of the first gas giant planet at this location in the solar system (Ida & Lin 2004).

During the final stage of disk depletion, the snow line moves into the optically thin region. For a 1 $M_\odot$, 1 $L_\odot$ T Tauri star this transition occurs when $\dot{M}$ drops below $2 \times 10^{-10}\ M_\odot\ \mathrm{yr}^{-1}$. Note that the sharpness of the transition observed in Figure 7 may be an artifact of the simplistic snow line model used here; we will study the physics of the snow line and the consequences of the transition from optically thick to optically thin in more detail in a subsequent paper.

Most interestingly, we find that the position of the snow line drops down to a radius of about 0.6 AU before expanding out again. This location is comparable to the inner boundary of the habitable zone around solar-type stars (Kasting et al. 1993). Our finding is the first to suggest a very close-in snow line for disks in which accretional heating is self-consistently taken into account. While earlier work by Sasselov & Lecar (2000) found that passive disks, i.e., with no accretional heating, could sustain a snow line as far in as perhaps 1 AU for solar-type stars, it is not clear that the passive disk approximation is appropriate when modeling T Tauri stars.

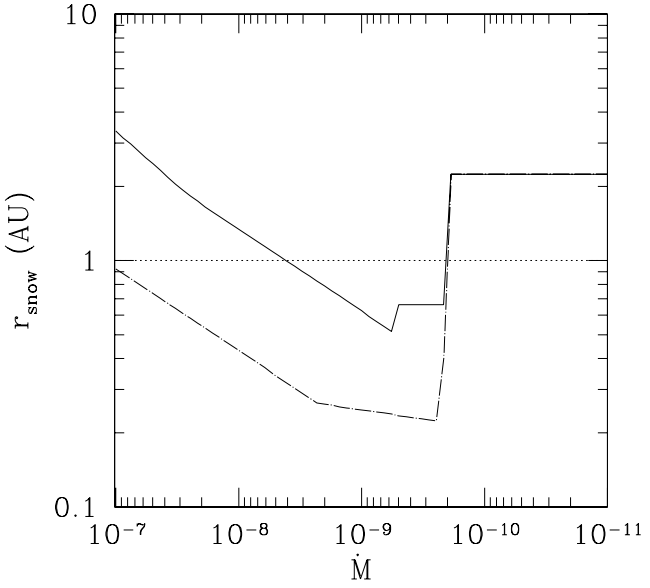

FIG. 7.—Variation of the position of the snow line as a function of mass accretion rate for a 1 $M_\odot$, 1 $L_\odot$ T Tauri star. The solid line represents the location where the midplane temperature $T_m = 160$ K, whereas the dot-dashed line represents that where the effective temperature $T_e = 160$ K. Between these two locations, ice can retain solid phase in a fraction of the disk near its surface. Since a large fraction of the grains are located near the midplane, along with the turbulent gas, the ice line for the midplane temperature is more relevant for determining the phase of most water molecules. The slow decrease in the position of the snow line (for T_m) as $\dot{M}$ initially decreases corresponds to the phase in which the snow line is located in the strongly opaque region. The first plateau in this profile arises when the snow line moves into the weakly opaque region. Therefore, the observed jump is an artifact of the mathematical asymptotics and should be interpreted instead as a smooth flattening of the profile. The second plateau, however, corresponds to the genuine physical transition of the snow line moving from the optically thick to the optically thin region as the disk depletes.

More recent work by Lecar et al. (2006) includes self-consistent calculations of the position of the snow line in the case of quasi-steady accreting disks around solar-type stars, for various values of the total mass accretion rate. The principal difference with our paper is that they fix the surface density of the disk and allow for a nonconstant α, while we fix α and calculate the surface density of the disk. Comparing both sets of results for the same mass accretion rates, we find that the snow line positions found are consistent within 10%–20%, ours being systematically slightly lower. Note that they do not calculate disk models for accretion rates lower than $\dot{M} = 10^{-8}\ M_\odot\ \mathrm{yr}^{-1}$; it will be interesting to see what is the minimum radius of the snow line in their calculations before transition into the optically thin regime.

The consequences of our finding are potentially far reaching. When the disk mass accretion rate has declined to about $5 \times 10^{-9}\ M_\odot\ \mathrm{yr}^{-1}$, the snow line crosses the Earth's orbit and steadily continues shrinking; at this point, the local total surface density of the disk is about 400 g cm^{-2}, so that in a ring of width $x r_{\mathrm{hill}}$ around the Earth's orbit one may find about $2 \times 10^{-2} x\ M_\oplus$ of condensed water in the form of icy particles. About half this amount in ices is also found around the orbit of Venus when the snow line crosses its orbit. This amount largely exceeds the current

total water content of Earth and Venus and could provide an alternative explanation for their hydration: the possibility of a late-stage accretion of ice grains onto large protoplanetary embryos in situ has the main advantage of providing a simple deterministic explanation for the measured D/H abundance ratio (Lunine 2005) of the oceans' water.

Finally, we also note that T Tauri stars younger than 1 Myr undergo FU Orionis outbursts (Herbig 1977; Hartmann & Kenyon 1985). During these outbursts, the central luminosity increases above 100 $L_\odot$ (Hartmann 2001) and the snow line can nearly instantly expand well beyond 100 AU, then retreat back to its initial position in a short period of time ($\sim$100 yr). This episodic relocation of the snow line will clearly be very disruptive to the growth of any icy body in most regions of the disk within the first 10^5 yr of the disk's evolution. This phenomenon may be observable through the coexistence of water vapor and ice at large radii in very young protostellar disks.

We thank T. Guillot, K. Kretke, C. Lada, S. Mohanty, G. Ogilvie, J. Pringle, and A. Youdin for useful conversations. This work was supported in part by NASA (NAGS5-11779, NNG06-GF45G, NNG04G-191G), JPL (1270927), NSF (AST 05-07424), and the California Space Institute.

APPENDIX

This appendix contains some of the mathematical tools and supplements used toward the derivation of many of the equations from this paper.

1. *Basic asymptotic integration method*.—Suppose we attempt to integrate a function $e^{-f(x)}$ within the interval $[a, b]$, when $f(x)$ has a minimum at $x = a$. Then

$$\int_a^b e^{-f(x)}\,dx \simeq \int_a^b e^{-f(a)-(x-a)f'(a)}\,dx = e^{-f(a)}\int_0^{b-a} e^{-uf'(a)}\,du = \frac{e^{-f(a)}}{f'(a)}\left(1-e^{-(b-a)f'(a)}\right) \simeq \frac{e^{-f(a)}}{f'(a)}, \tag{A1}$$

in the limit where $(b-a)f'(a) \gg 1$. Naturally, the curvature terms neglected in the expansion of $f(x)$ near $x = a$ also set another condition on the applicability of the approximation that must be checked for self-consistency.

When $b \to +\infty$, this approximation can be used, for instance, to recover the well-known approximation to the complementary error function as $x \to +\infty$:

$$\mathrm{erfc}\,(x) = \frac{2}{\sqrt{\pi}}\int_x^{+\infty} e^{-u^2}\,du \simeq \frac{1}{\sqrt{\pi}}\frac{e^{-x^2}}{x}. \tag{A2}$$

This approximation is used in the derivation of equation (23).

2. *Position of the superheated layer*.—The derivation of equation (17) is straightforward using this method. Indeed,

$$\int_0^r \tilde{Z}\kappa_V \rho(z', r')\,d\boldsymbol{l} = \kappa_V \int_0^r \rho_m(r') e^{-\left(z_s^2/r^2\right)\left[r'^2/2h^2(r')\right]}\,dr', \tag{A3}$$

so that we can use the above method with

$$a = 0, \qquad b = r, \tag{A4}$$

$$f(r') = \frac{z_s^2}{r^2}\frac{r'^2}{2h^2(r')} - \ln\left[\tilde{Z}\rho_m(r')\right] \tag{A5}$$

(note that we thereby consider the possibility of $\tilde{Z}$ having a slow variation with r). Here the function $f(r')$ has a minimum at $r' = b$ provided that the disk is flaring (i.e., provided that h/r is an increasing function of r). In that case, the formula used is

$$\int_a^b e^{-f(x)}\,dx \simeq \frac{e^{-f(b)}}{-f'(b)} \tag{A6}$$

instead, yielding equation (17) a few algebraic manipulations later.

The calculation of the exact position of the superheated layer in the limit where the disk is optically thick and the derivation of equations (53) and (54) are slightly more involved. To begin with, let us rewrite the gas density above the photosphere in this region as

$$\rho(r, z) = \rho_e(r) e^{-\left(z^2-z_e^2\right)/2h_e^2}, \tag{A7}$$

where $\rho_e(r)$ is the density at the photosphere,

$$\rho_e(r) = \rho_m(r)\left(1-\frac{z_e^2}{H^2}\right)^n. \tag{A8}$$

The equivalent calculation and manipulations that were used to obtain equation (17) in the optically thin case can be used again to yield this time

$$\tilde{Z}\rho_e h_e \kappa_V e^{-\left(z_s^2-z_e^2\right)/2h_e^2} = \frac{z_s^2}{h_e^2} r \frac{d}{dr}\left(\frac{h_e}{r}\right) + \frac{h_e}{r}\frac{d\ln\left(\tilde{Z}\rho_e\right)}{d\ln r} + h_e \frac{d}{dr}\left(\frac{z_e^2}{2h_e^2}\right). \tag{A9}$$

In the limit of a strongly opaque disk, $z_s \gg h_e$ and $z_e \gg h_e$ (in other words, the atmosphere is much colder than the midplane), so that we can simplify the above by neglecting the second term on the right-hand side compared to the others. Now we use equation (43) to simplify this to

$$\tilde{Z}\rho_e h_e \kappa_V e^{-\left(z_s^2-z_e^2\right)/2h_e^2} = \frac{\theta^2}{\varepsilon_e^{1/2}}\alpha, \tag{A10}$$

where α is defined by equation (18).

On the other hand, the total surface area of grains above the superheated layer is given by

$$A_s = \tilde{Z}\rho_e \kappa_V e^{-\left(z_s^2-z_e^2\right)/2h_e^2}\frac{h_e^2}{z_s}, \tag{A11}$$

so that

$$A_s = \frac{\theta^2}{\varepsilon_e^{1/2}}\alpha\frac{h_e}{z_s} = \frac{z_s}{h}\alpha \tag{A12}$$

on the assumption (which is proved below) that $z_s \sim H$.

To prove that $z_s \sim H$ in the limit of a strongly opaque disk, we construct the quantity

$$\delta = \frac{z_s^2 - z_e^2}{H^2}, \tag{A13}$$

so that equation (A10) can be rewritten as

$$\tilde{Z}\rho_m \epsilon^n \kappa_V e^{-\left(\theta^2/2\epsilon\right)\delta} = \frac{\theta^2}{\varepsilon_e}\frac{\alpha}{H}, \tag{A14}$$

which can be solved for δ as

$$\delta = \frac{2\epsilon}{\theta^2}\ln\left(\frac{\epsilon^{n+1}\tilde{Z}\kappa_V\rho_m H}{\alpha\theta^2}\right) = \frac{2\epsilon}{\theta^2}\ln\left[\frac{\epsilon^{n+1}\tau_V^{\rm tot}}{I(n)\alpha\theta^2}\right], \tag{A15}$$

which shows that δ is proportional to ϵ, or in other words that z_s is close to H when z_e is close to H.

3. *Radial structure of the disk.*—When solving for the radial structure of the disk, we are always integrating ordinary differential equations of the kind

$$\frac{d}{dr}\left(\frac{h}{r}\right) = B\left(\frac{h}{r}\right)^a r^b, \tag{A16}$$

for which the general mathematical solution is

$$\left(\frac{h}{r}\right) = \left(K + \frac{1-a}{b+1}Br^{b+1}\right)^{1/(1-a)}. \tag{A17}$$

However, it is possible to set the integrating constant K to zero on physical grounds, since it would otherwise correspond to an unphysical constant heating source in the disk. Once this is done, we simply get

$$h = \left(\frac{1-a}{b+1}B\right)^{1/(1-a)} r^{(b+1)/(1-a)+1}. \tag{A18}$$

REFERENCES

Adachi, I., Hayashi, C., & Nakazawa, K. 1976, Prog. Theor. Phys., 56, 1756
Adams, F. C., Lada, C. J., & Shu, F. H. 1987, ApJ, 312, 788
Balbus, S. A, & Hawley, J. F. 1991, ApJ, 376, 214
Beckwith, S. V. W., & Sargent, A. I. 1991, ApJ, 381, 250
———. 1996, Nature, 383, 139
Bell, K. R. 1999, ApJ, 526, 411
Calvet, N., D'Alessio, P., Hartmann, L., Wilnet, D., Walsh, A., & Sitko, M. 2002, ApJ, 568, 1008
Chiang, E. I., & Goldreich, P. 1997, ApJ, 490, 368 (CG97)
Ciesla, F. J., & Cuzzi, J. N. 2006, Icarus, 181, 178

D'Alessio, P., Calvet, N., & Hartmann, L. 2001, ApJ, 553, 321
Dubrulle, B., Marie, L., Normand, C., Richard, D., Hersant, F., & Zahn, J. P. 2005, A&A, 429, 1
Dullemond, C. P., & Dominik, C. 2004, A&A, 417, 159
Dullemond, C. P., Hollenback, D., & Kamp, I., & D'Alessio, P. 2006, in Protostars and Planets V, in press
Gammie, C. F. 1996, ApJ, 457, 355
Garaud, P., & Lin, D. N. C. 2004, ApJ, 608, 1050
Goldreich, P., & Ward, W. R. 1973, ApJ, 183, 1051
Gomez, G. C., & Ostriker, E. C. 2005, ApJ, 630, 1093
Gradshteyn, I. S., & Rhyshik, I. M. 1980, Table of Integrals, Series and Products (New York: Academic)
Greaves, J. S., et al. 2005, ApJ, 619, L187
Hartmann, L. 2001, Accretion Process in Star Formation (Cambridge: Cambridge Univ. Press)
Hartmann, L., & Kenyon, S. J. 1985, ApJ, 299, 462
Hayashi, C., Nakazawa, K., & Nakagawa, Y. 1985, in Protostars and Planets II , ed. D. Black & M. Mathews (Tucson: Univ. Arizona Press), 1100
Herbig, G. H. 1977, ApJ, 217, 693
Ida, S., & Lin, D. N. C. 2004, ApJ, 604, 388
Kasting, H. F., Whitmire, D. P., & Reynolds, R. T. 1993, Icarus, 101, 108
Lada, C. J., et al. 2006, AJ, 131, 1574
Laplace, P. S. de 1796, Exposition du Système du Monde (Paris)
Lecar, M., Podolak, M., Sasselov, D., & Chiang, E. 2006, ApJ, 640, 1115
Lin, D. N. C., & Papaloizou, J. C. B. 1980, MNRAS, 191, 37
———. 1985, in Protostars and Planets II, ed, D. Black & M. Mathews (Tucson: Univ. Arizona Press), 981
Looney, L. W., Mundy, L. G., & Welch, W. J. 2003, ApJ, 592, 255
Lunine, J. 2005, in Meteorites and the Early Solar System II, ed. D. Lauretta, L. A. Leshin, & H. Y. McSween, Jr. (Tucson: Univ. Arizona Press), 309
Lynden-Bell, D., & Pringle, J. E. 1974, MNRAS, 168, 603
Marcy, G. W., Cochran, W. D., & Mayor, M. 2000, in Protostars and Planets IV, ed V. Mannings, A. P. Boss, & S. S. Russell (Tucson: Univ. Arizona Press), 1285
Mathis, J. S., Rumpl, W., & Nordsieck, K. H. 1977, ApJ, 217, 425
McCabe, C., Duchene, G., & Ghez, A. M. 2003, ApJ, 588, L113
Morfill, G. E., & Voelk, H. J. 1984, ApJ, 287, 371
Mundy, L. G., Looney, L. W., & Welch, W. J. 2000, in Protostars and Planets IV, ed. V. Mannings, A. P. Boss, & S. S. Russell (Tucson: Univ. Arizona Press), 355
Quillen, A. C. 2002, AJ, 124, 400
Rafikov, R. R., & De Colle, F. 2006, ApJ, 646, 275
Richard, D., & Zahn, J. P. 1999, A&A, 347, 734
Ruden, S. P., & Lin, D. N. C. 1986, ApJ, 308, 883
Sasselov, D. D., & Lecar, M. 2000, ApJ, 528, 995
Shen, Z.-X., Jones, B., Lin, D. N. C., Liu, X.-W., & Li, S.-L. 2005, ApJ, 635, 608
Shuping, R. Y., Bally, J., Morris, M., & Throop, H. 2003, ApJ, 587, L109
Supulver, K. D., & Lin, D. N. C. 2000, Icarus, 146, 525
Takeuchi, T., & Lin, D. N. C. 2002, ApJ, 581, 1344
———. 2005, ApJ, 623, 482
Watanabe, S., Nakagawa, Y., & Nakazawa, K. 1990, ApJ, 358, 282
Weidenschilling, S. J. 1977, MNRAS, 180, 57
Weidenschilling, S. J., & Cuzzi, J. N. 1993, in Protostars and Planets III, ed. E. H. Levy & J. I. Lunine (Tucson: Univ. Arizona Press), 1031
Wilden, B. S., Jones, B. F., Lin, D. N. C., & Soderblom, D. R. 2002, AJ, 124, 2799
Youdin, A. N, & Chiang, E. 2004, ApJ, 601, 1109